**Project 1** - Dissecting the role of acquired regions of homozygosity detected by microarray along the genome of a large cohort of adult patients with B-cell precursor acute lymphoblastic leukemia

**Project 2**- Unveiling the genetic landscape of B-cell precursor acute lymphoblastic leukemia by novel technologies: optical genome mapping versus digital multiplex ligation dependent-probe amplification

PhD School in Innovation in Immune-mediated and Hematological Disorders

Curriculum Hematology

37th cycle

Director: Prof. Silvano Sozzani

PhD supervisor

Prof. Ilaria Del Giudice

PhD candidate

Dr. Gianfranco Lapietra

(ID number 1406398)

Co-supervisors

Prof. Sabina Chiaretti

Prof. Josep Maria Ribera

INDEX

1. Introduction: Genetic landscape of adult B-cell precursor acute lymphoblastic leukemia

**Project 1** - Dissecting the role of acquired regions of homozygosity detected by microarray along the genome of a large cohort of adult patients with B-cell precursor acute lymphoblastic leukemia

**Project 2**- Unveiling the genetic landscape of B-cell precursor acute lymphoblastic leukemia by novel technologies: optical genome mapping versus digital multiplex ligation dependent-probe amplification

Genetic landscape of adult B-cell precursor acute lymphoblastic leukemia

## 1.1 Definition and epidemiology

B-cell precursor acute lymphoblastic leukemia (B-ALL) is a very heterogeneous hematologic malignancy, characterized by the clonal expansion of immature lymphoid precursors spreading from the bone marrow (BM) into the bloodstream, possibly involving other lymphoid and non-lymphoid organs. Over 50% of cases is diagnosed under the age of 20, being B-ALL the most recurrent form of childhood leukemia. By contrast, it represents only 20% of leukemias among adults (1).

## 1.2 Diagnostic work-up

Morphology, multi-color flow cytometry (MFC) and molecular genetics on samples from BM aspirate are required for confirmation of diagnostic suspicion (2). B-ALL is defined by >20% of myeloperoxidase-negative blasts with typical morphology infiltrating BM. According to the French-American-British (FAB) classification, three different categories of B-ALL can be described, based on morphologic findings (3):

L1: it is characterized by small cells with regular nuclear shape, homogeneous chromatin, small or absent nucleolus and scanty cytoplasm;

L2: it includes larger blasts with irregular nuclear shape, heterogeneous chromatin, prominent nucleolus and more cytoplasm;

L3: in this group, the cells are very large and rich in vacuoles, nucleus is often regular with nucleolus and the cytoplasm is abundant.

CD19, CD22 and CD79a are the crucial markers to be detected by MFC for proper assignment to B-lineage. The immunophenotypic characterization should be further extended to define the differentiation stage, according to the European Group for the Immunological Characterization of Leukemias (EGIL) classification (4):

Pro-B:  it is characterized by expression of CD19, CD79a and CD22 in the absence of CD10;

Common: it is defined by concomitant expression of the above-mentioned crucial markers and CD10;

Pre-B: the cells exhibit cytoplasmic immunoglobulin M (cIgM) while surface Ig (sIg) is negative;

Mature: it is characterized by expression of both sIg and of CD20.

The routine genetic characterization relies on karyotyping, fluorescent in-situ hybridization (FISH) and reverse transcription polymerase chain reaction (RT-PCR). However, in the recent years other techniques such as multiplex ligation dependent-probe amplification (MLPA), single nucleotide polymorphism (SNP) array or next-generation sequencing (NGS) (mainly gene panels) are increasingly being incorporated in the routine testing upfront.

1.3 Genetic characterization

B-ALL is caused by a multistep oncogenic process led by progressive accretion of genomic lesions: the initial event is assumed to be a major chromosomal abnormality but further aberrations are required for leukemia development.

Primary genetic abnormalities:

Many driver alterations underlying leukemogenesis have been identified (5):

- t(9;22)(q34;q11.2): it is the most frequent aberration in the adult population, leading to the presence of Philadelphia (Ph) chromosome and therefore to *BCR::ABL1* fusion transcript with constitutional activation of survival signals. Thanks to the recent introduction of tyrosine kinase inhibitors (TKIs), the unfavourable outcome of this translocation has been partly overcome (6);
- *KMT2A* rearrangements: translocations involving this methyltransferase at 11q23 are mostly described in infants and adults and associated with a dismal prognosis. *KMT2A* may translocate to several loci but 90% of rearrangements involve *AFF1*, *MLLT1*, *MLLT3*, located on 4q21, 19p13.3, 9p21.3, respectively (7);
- t(12;21)(p13;q22): this translocation is more frequent in children than in adult patients. It results in *ETV6::RUNX1* fusion transcript with good impact on prognosis (8);
- *TCF3* rearrangements: *TCF3* is a transcription factor on 19p13 that could translocate next to *PBX1* or *HLF*, on 1q23 and 17q21, respectively. t(1;19)(q23;p13) is detected in approximately 7% of children patients and associated with intermediate prognosis (9). t(17;19)(q21;p13) is rare among adults and implies high relapse and death rates (10);
- intrachromosomal amplification of chromosome 21 (iAMP21): this aberration is defined by an increased number of signals (≥5) with *RUNX1* probe on 21q22 and is associated with unfavourable outcomes, which can be further improved with higher intensity treatments (11);
- ploidy variations: B-ALL may present with either an increase or a reduction in chromosomes number. High-hyperdiploidy is defined by a karyotype with at least 51 up to 65 chromosomes. It is usually detected in children and characterized by a good response to standard treatment (12). By contrast, low-hypodiploidy/near-triploidy is a very aggressive subtype of adult B-ALL, detected in up to 10% of cases. This form is characterized by <40 chromosomes and always associated with monoallelic loss of *TP53* and mutation of the remaining allele (13). Finally, near haploid ALL accounts for <30 chromosomes and is also related with poor outcome;
- Ph-like aberrations: Ph-like B-ALL have a similar gene expression profile as Ph+ counterpart, but lacking the typical t(9;22)(q34;q11.2). A wide variety of genetic lesions underlies this group for which at least three subtypes have been recently identified: *ABL1*-class rearranged; JAK-STAT

activated and not otherwise specified (NOS) (14). The first group includes all fusions involving *ABL1*, *ABL2*, *CSF1R* and *PDGFRB* with major sensitivity to TKIs. By contrast, the second group is characterized by hyper-activation of the JAK-STAT pathway. In most cases, this is due to *CRLF2* (Xp22.3) rearrangements to *IGH* (14q32.33) or *P2RY8* (Xp22.3). Other rarer aberrations are those involving *JAK2* (9p24.1), *EPOR* (19p13.2) and *IL7R* (5p13.2). NOS subtype encompasses alterations of kinase receptors and cytokines which are not embraced by the two main groups, such as *FLT3* (13q12.2), *FGFR1* (8p11.23), *NTRK3* (15q25.3) and *PTK2B* (8p21.2). Responsiveness of both Ph-like B-ALL JAK-STAT activated and NOS to TKIs or JAK-inhibitors is questionable (15).

- t(5;14)(q31.1;q32.3): this very rare chromosomal anomaly leads to the fusion product *IGH::IL3* with increased release of mature eosinophils in the peripheral blood and subsequent typical symptoms. Due to paucity of data, little is known about the evolution of this disease even if an intermediate prognosis has been highlighted by some case-series (16);

- other defined genetic abnormalities: across the last years, the use of omics techniques has allowed the identification of many other recurrent aberrations (5). Some of these novel alterations are associated to a good prognosis, such as *DUX4* (4q35.2) and *NUTM1* (15q14) rearrangements. Other alterations are burdened with poor prognosis. Among these, it is worth mentioning the rearrangements of *MEF2D* (1q22), *MYC* (8q24.21) and the cases with concomitant deletion at 13q12.2 and 17q21.31 leading to *CDX2* and UBTF deregulation, respectively (17). The role of several other alterations is still being investigated. To date, more recurrent aberrations with variable prognosis are *ZNF384* (12p13.31) rearrangements (18) and missense mutations affecting *PAX5* (9p13.2) (19) and *IKZF1* (7p12.2) (20).

- "like" subtypes: beyond Ph –like B-ALL, other cases with a gene expression profile resembling that of well-known categories in the absence of the driver aberration have been described: *ETV6-RUNX1*-like group is enriched with *ETV6* and *IKZF1* alterations (21); *KMT2A*-like cases are characterized by alterations affecting *AFF1* (4q21) and *HOXA9* (7p15.2) (22), while the category *ZNF384*-like includes recurrent *ZNF362* (1p35.1) fusions (23).

Recently, most of these subtypes have been included in both the World Health Organization (WHO) and International Consensus (IC) classifications (Table 1) (24, 14). The differences between the two classifications account for the variability of B-ALL genetic landscape.

Table 1- Comparison between B-ALL WHO classification, 5<sup>th</sup> edition, and ICC classification

| WHO classification, 5th edition | ICC classification |
|---|---|
| B-lymphoblastic leukaemia/lymphoma, NOS | B-ALL without recurrent genetic abnormalities |
| B-lymphoblastic leukaemia/lymphoma with high hyperdiploidy | B-ALL, hyperdiploid |
| B-lymphoblastic leukaemia/lymphoma with hypodiploidy | -B-ALL, low hypodiploid; <br> -B-ALL, near haploid |
| B-lymphoblastic leukaemia/lymphoma with iAMP21 | B-ALL with iAMP21 |
| B-lymphoblastic leukaemia/lymphoma with *BCR::ABL1* fusion | B-ALL with t(9;22)(q34.1;q11.2)/*BCR::ABL1*: <br> - with lymphoid only involvement; <br> - with multilineage involvement |
| B-lymphoblastic leukaemia/lymphoma with *BCR::ABL1*-like features | -B-ALL, *BCR::ABL1*-like, ABL-1 class rearranged; <br> - B-ALL, *BCR::ABL1*-like, JAK-STAT activated; <br> - B-ALL, *BCR::ABL1*-like, NOS |
| B-lymphoblastic leukaemia/lymphoma with *KMT2A* rearrangement | B-ALL with t(v;11q23.3)/*KMT2A* rearranged |
| B-lymphoblastic leukaemia/lymphoma with *ETV6::RUNX1* fusion | B-ALL with t(12;21)(p13.2;q22.1)/*ETV6::RUNX1* |
| B-lymphoblastic leukaemia/lymphoma with *ETV6::RUNX1*-like features | B-ALL, *ETV6::RUNX1*-like (provisional entity) |
| B-lymphoblastic leukaemia/lymphoma with *TCF3::PBX1* fusion | B-ALL with t(1;19)(q23.3;p13.3)/*TCF3::PBX1* |
| B-lymphoblastic leukaemia/lymphoma with *IGH::IL3* fusion | B-ALL with t(5;14)(q31.1;q32.3)/*IL3::IGH* |
| B-lymphoblastic leukaemia/lymphoma with *TCF3::HLF* fusion | B-ALL with *HLF* rearrangement |
| B-lymphoblastic leukaemia/lymphoma with other defined genetic abnormalities | -B-ALL with *MYC* rearrangement; <br> -B-ALL with *DUX4* rearrangement; <br> -B-ALL with *MEF2D* rearrangement; <br> -B-ALL with *ZNF384* rearrangement; <br> -B-ALL with *NUTM1* rearrangement; <br> -B-ALL with *UBTF::ATXN7L3/PAN3, CDX2* ("CDX2/UBTF"); <br> -B-ALL with IKZF1 N159Y; <br> -B-ALL with PAX5 P80R |
| | Provisional entities: <br> -B-ALL, with PAX5 alteration; <br> -B-ALL, with mutated ZEB2 (p.H1038R)/*IGH::CEBPE*; <br> -B-ALL, *ZNF384* rearranged-like; <br> -B-ALL, *KMT2A* rearranged-like |

Abbreviation:

NOS: not otherwise specified; iAMP21: chromosome 21 intrachromosomal amplification.

Secondary genetic abnormalities:

Most of the additional aberrations described in leukemogenesis are copy-number variations (CNVs) affecting genes involved in B-lineage lymphoid differentiation and proliferation control:

- *EBF1* (5q33.3): it is a transcription factor cooperating for the activation of B-cell specific genes during the lineage commitment;
- *IKZF1* (7p12.2): it is a DNA-binding protein with a zinc-finger domains through which it modulates the lymphocyte differentiation;
- *PAX5* (9p13.2): this gene encodes the B-cell lineage specific activator protein which is required during the early stages of B-cell differentiation;
- *CDKN2A/B* (9p21.3): it codes for three tumour suppressor proteins, p16 and p14arf (*CDKN2A/B*), and p15 (*CDKN2B*), involved in the regulation of cell cycle by activation of retinoblastoma proteins and p53, respectively;
- *ETV6* (12p13.2): it codes for a transcription factor active in hematopoiesis;
- *BTG1* (12q21.33): due to its variable expression during different phases of the cell cycle, it is thought to play a central role in the control of proliferation and response to glucocorticoids;
- *RB1* (13q14.2): it is a negative regulator of the G1/S transition of the cell cycle;
- sexual pseudo autosomal region 1 (PAR1): it is a five Mb region in the p telomeric region of X and Y-chromosomes. Many genes coding for proteins involved in JAK-STAT pathway map in this region.

The identification of a universal prognostic role for any CNV is challenging due to the recurrent association with primary alterations. In 2014, Moorman et al. developed and validated a score for pediatric B-ALL risk-stratification based both on typical cytogenetic aberrations and on the copy-number status of the eight genes mentioned above. This system revealed two subgroups with different outcomes: the good-risk group including *ETV6::RUNX1*, high hyperdiploidy, normal copy-number status for all eight genes, isolated deletions affecting *ETV6*/*PAX5*/*BTG1*, *ETV6* deletions with a single additional deletion of *BTG1*/*PAX5*/*CDKN2A/B*, and the poor risk group including any other aberration (25). However, the role of CNVs was proven to be more complex than expected with the introduction of omics technique and a more extensive assessment of genetic landscape. In particular, the so-called *IKZF1*^plus profile was identified by merging genetic features and clinical outcome of 991 pediatric patients from Italian and German trials: the co-occurrence of *IKZF1* deletion with deletions in *CDKN2A*, *CDKN2B*, *PAX5*, or *PAR1* in the absence of *ERG* (21q22.2) deletion defines a subset of intermediate and high-risk patients with a very poor outcome (26).Several efforts were made to understand whether the unfavourable impact of these CNVs was also maintained in the adult population. For instance, deletions of *EBF1*, *IKZF1* and *CDKN2A/B* were confirmed to negatively affect the prognosis in a large cohort of Spanish adolescent and adult patients (27). In a following report by the same group, *IKZF1* and *CDKN2A/B*

were identified as markers of disease recurrence, the latter being associated with minimal residual disease (MRD) persistence (28). The Italian cooperative group also confirmed the prognostic value of these CNVs within a large cohort of age-stratified B-ALL cases, proving that patients harbouring deletions of *CDKN2A/B* and *EBF1* had shorter disease-free survival than those wild-type (29). They also showed that deletions affecting *IKZF1*, *BTG1* and *EBF1* are significantly more frequent in Ph-like subtype (30) and confirmed the adverse impact of *IKZF1*[plus] profile in a cohort of Ph+ B-ALL patients treated with upfront chemo-free approach (31, 32). More recently, the European Working Group for adult ALL (EWALL) proposed a robust and integrated prognostic index for risk stratification in adult ALL, using data from four large clinical trials (33). This score takes into account MRD value at the end of induction, total leukocyte count at baseline and specific genetic alterations: good-risk aberrations include t(12;21)(p13;q22), high-hyperdiploidy and *ZNF384* fusions; while *KMT2A* fusions, both low-hypodiploidy and near-haploidy, iAMP21, JAK-STAT aberrations and complex karyotype (defined as ≥5 abnormalities detected by standard karyotyping) are considered as high-risk hallmarks. CNVs are not considered: a consensus view on their incorporation into stratification algorithms is still lacking.

## 1.4 Mechanisms of genetic aberrations

As for most hematologic and non-hematologic malignancies, the pathogenesis of B-ALL is multifactorial. Therefore, despite the continuous efforts by multiple cooperative groups, the exact mechanisms are still far to be fully elucidated. Certainly, the double-hit hypothesis by Knudson is also valid in the case of ALL: its development is possible when in a subject both alleles of one or more genes undergo an alteration (34). The occurrence of double hit may be spontaneous or facilitated by predisposing factors, such as inherited genetic alterations and environmental factors (35). Constitutional syndromes (e.g. Down syndrome, Fanconi anemia, ataxia-teleangectasia), constitutional abnormalities of chromosome 21 [e.g. rob(15;21)(q10;q10)c, r(21)c] and some SNPs are universally recognized as contributing to B-ALL (36). On the other side, pesticide exposure, ionizing radiations and recurrent childhood infections are the most frequent environmental factors involved in leukemogenesis, as suggested by epidemiologic data (37).

The action of the hits, whether spontaneous or induced, may occur in any of the phases of the cell cycle: a perturbation during the S phase could result in a single-nucleotide mutation; by contrast, a damage in the M phase will manifest either by nondisjunction or by breaking and rearranging chromosomes (38). For these damages to be maintained, a malfunction of the repair mechanisms is also required. Indeed, the chromosome mis-segregation is kept only in presence of defects also affecting correction mechanisms. Under physiologic conditions, this machinery acts by removing defective attachments via destabilization of microtubules at kinetochore (39). Even in the case of a correction failure due to a transitory and stochastic malfunction of this apparatus, checkpoints in the phases following separation would induce a reduction in cell-fitness, with subsequent death. Therefore, chromosomal instability (CIN) as a co-responsible for cancer is a complex phenomenon characterized by the progressive accretion of errors at different levels of cell survival control.

From a cyto-genomic point of view, CIN could manifest in two different forms (40):

- numerical CIN
- structural CIN

Numerical CIN is characterized by a change in the normal ploidy of a cell (2n). This variation may be due to gains and losses of either individual whole chromosomes (aneuploidy) or sets of chromosomes (hyper- and hypo ploidy, respectively).

Structural CIN is associated to gains and losses of chromosome segments. In most cases, these aberrations do not imply any alteration of normal cellular 2n state:

- inversion: it occurs when a double break happens within a chromosome arm and the resulting segment re-enters the same arm with opposite orientation to the initial one;

- deletion: it is the loss of a chromosome segment which may be more or less wide;
- amplification: it is any duplication of a chromosome segment, often associated to the acquisition of multiple copies of the same gene;
- balanced translocation: it is characterized by a fair exchange of material between non-homologous chromosomes. This switching could lead to the formation of fusion genes resulting in aberrant protein synthesis.

With less frequency, structural CIN is associated to a ploidy change, i.e. unbalanced translocations between 2 chromosomes. The product of this aberration is a derivative chromosome replacing the parts of the 2 involved chromosomes that are missed. If this event involves the acrocentric chromosomes, a Robertsonian translocation is identified. In this case, the remaining short arms are lost.

We may consider uniparental disomy (UPD) as a peculiar form of CIN: even if it does not imply a ploidy change, it is associated to the loss of one of the two alleles of one or more genes with potential consequences on the proper functioning of the genomic machine.

## 1.5 Novel challenges

Over the years, the identification of all the above-mentioned genetic aberrations and the subsequent refinement of treatment-backbone has led to a general improvement of prognosis. However, a striking difference across the age-subgroups still exists. Indeed, while about 90% of children are alive 5 years after B-ALL diagnosis, the adult population still suffers from poor outcome, with long-term survival rates around 50% (41, 42). The dramatic variation in response relies on age-related fragility (i.e. comorbidity, reduced compliance to treatment, high rate of iatrogenic side effects) but also on the different biology of the disease depending on the age of onset. As mentioned above, high-risk aberrations are more frequently detected in the adult population. Furthermore, none of the known driver genetic alterations defined by standard cytogenetic testing can be identified in a non-negligible percentage of cases. A comprehensive genetic and genomic analysis performed on 210 samples collected within multicentre British trials showed that 32% of patients remain uncharacterized and provisionally defined as B-other (43).

Therefore, two different needs are unmet:

- Identification of novel genetic aberrations beyond the well-known driver alterations (project 1);
- Validation and implementation of novel technologies for a more extensive evaluation of adult B-ALL genetic landscape (project 2).

**Project 1:** Dissecting the role of acquired regions of homozygosity detected by microarray along the genome of a large cohort of adult patients with B-cell precursor acute lymphoblastic leukemia

ABSTRACT

**INTRODUCTION**

Acquired regions of homozygosity (aROHs) detected along the genome are due to mitotic recombination between homologous chromosomes. This mechanism may contribute to the growth of a neoplastic clone if the involved region embraces tumor suppressor or onco-genes harbouring a mutation, with subsequent loss of the wild-type allele and duplication of the aberrant one. Cytogenetic diagnostic tools based on allelic load assay has allowed identification of aROHs also in B-cell acute lymphoblastic leukemia (B-ALL). However, real-life data about contribution of these aberrations to leukemogenesis are scarce and controversial.

**AIM**

We investigated aROHs detected in a large and uniform longitudinal cohort of adult B-ALL patients (pts), to define their potential role.

**METHODS AND RESULTS**

The study was carried out at Josep Carreras Leukemia Research Institute (Badalona, ES). Pts enrolled in clinical trial NCT04179929 with available single nucleotide polymorphisms (SNP)-array analysis performed at baseline for genetic risk-stratification as per protocol were considered evaluable. For each patient, DNA extracted from infiltrated bone marrow (BM) and amplified by PCR was hybridized to GeneChip Mapping 750 K array (Affymetrix, Santa Clara, US). Hybridization to each probe was assessed using a GeneChip Scanner (Affymetrix) and results scored using CHAS v4.5 software (Affymetrix). For the aim of the study, we first selected ROHs with size≥3 Mb and mapping in regions covered with≥20 consecutive probes. In order to identify only acquired non-polymorphic forms, we excluded ROHs overlapping ≥50% of their length with regions included in public databases of healthy controls and with variant of allele frequency (VAF)>BM infiltration. Finally, eligible calls were cross-referenced with pts' biological and clinical data for statistical analysis. From December 2019 to March 2024, 371 pts were included in LAL-19 trial. 277 cases (75%) were eligible for our study. Median age was 40 years (range 18-60). The male/female ratio was 1:1. Overall, 332 aROHs were detected in 156 pts (56%). The median number of aROHs per pt was one (range 1-9); the median size was 6.7 Mb (range 3-27.5). 94 % of aROHs were segmental. aROHs were distributed across the whole genome, 5q31.1 and 7q11.23 being the most frequently involved regions, without affecting any gene clearly involved in the leukemogenesis. No difference was observed between pts with and without aROHs in terms of age, sex and clinical features at the onset. However, the presence of aROHs was associated with the absence of hypodiploidy (<44 chromosomes) and absence of mutations in the survival regulatory pathways detected by NGS standard panel (p=0.029 and p=0.043, respectively). Based on follow-up (FU) data, survival analysis was possible in 192/277 pts (69%). After a median FU of one year, the presence of aROHs had no impact on either overall survival (OS) (p=0.594) or cumulative incidence of relapse (CIR) (p=0.893). Within the population with aROHs, no difference emerged in terms of OS and CIR stratifying by number (1 *versus* >1) and size of lesions (<20 Mb *versus* >20 Mb, being 20 Mb the most employed cut-off in literature).

**CONCLUSION**

Our study confirms recurrence of non-polymorphic aROHs along the genome of adult B-ALL pts, without affecting key-genes for leukemogenesis. These aberrations do not affect the prognosis. On the contrary, a protective role for the genome could be hypothesized, due to their association with a low rate of mutation and with preserved diploidy.

## 2.1 Uniparental disomy: definition and origin

We define UPD by the presence of 2 identical copies of a segment or whole chromosome derived from the same parent, leading to the so-called copy neutral loss of heterozygosity (CN-LOH). This phenomenon may occur at the germinal level, as a non-clonal event affecting the whole offspring, or at the somatic level, in the context of a clonal evolution, with neoplastic potential (Figure 1).

Figure 1- Classification of uniparental disomy
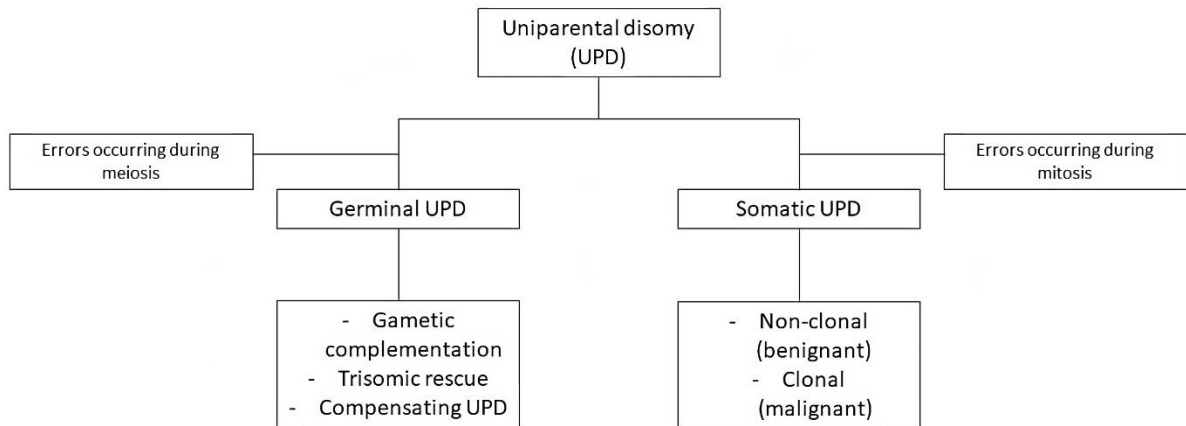
2.1.a Germinal uniparental disomy

Germinal UPD is due to mistakes during meiosis preceding the formation of gametes. Errors occurring during meiosis I lead to heterodisomy while those happening in the meiosis II are responsible for isodisomy. Heterodisomy is defined by the presence of both homologues of only one parent in the absence of the counterpart coming from the other parent. While isodisomy is characterized by two identical copies from one parental homologue. Overall, three main mechanisms have been recognized as leading to germinal UPD:

    -gametic complementation;

    -trisomic rescue;

    -compensatory UPD.

Gametic complementation happens when an egg with an extra chromosome is fertilized by a sperm missing that same chromosome, or vice-versa. It has been calculated that during the fertile life the percentage of aneuploid oocytes and spermatocytes produced is 18% and 3-4%, respectively. Any chromosome can be involved (44).

Trisomy rescue is a correction event aimed at eliminating supernumerary chromosome, which can result from the fertilization of a haploid egg by a diploid sperm or of a diploid egg by a haploid sperm. This event must occur at very early stages of embryonic development to be effective. Therefore, the trisomic lineage is only confined to the placenta in mosaicism. As this is a rather rare event, little is known about the mechanisms underlying the selection of the extra chromosome to be eliminated (45).

Compensatory UPD occurs when an abnormal or missing chromosome is replaced with a copy of the normal homologue that is obtained by bypassing sister chromatid segregation. The earlier the correction, the greater the adverse selection on the line with monosomy or abnormality and the greater the chance that it will be eliminated, with minimal consequences on the product of conception (46).

Overall, whatever the mechanism, germinal UPD is expected to happen in 1/80000 births, with a dramatic increase as the mother ages (47). Nevertheless, the cases in which germline UPD manifests with a pathological phenotype are minor, depending on the genomic area affected. Specifically, heterodisomy is associated with abnormalities if imprinted regions are involved. Imprinting is a phenomenon due to epigenetic silencing of a gene, based on parental origin. The presence of heterodisomic UPD for the silenced gene results in non-expression of the active counterpart with development of syndromes known as "genetic imprinting disorders", such as Prader-Willi and Angelman syndromes, caused by maternal and paternal UPD of chromosome 15q11-q13, respectively; Beckwith-Wiedemann syndrome (paternal UPD11p15.5), transient

neonatal diabetes (paternal UPD6p22.1 or 6q24.2), Russell-Silver syndrome (maternal UPD7) and `maternal UPD14' syndrome (48). On the other hand, isodisomy may imply the coexistence of two copies of a recessive mutation coming from a healthy carrier. Over time, many cases of genetic diseases transmitted as recessive trait have been associated to isodisomic UPD, e.g. cystic fibrosis, hemophilia A, spinal muscular atrophy III, congenital adrenal hyperplasia and multiple endocrine neoplasia type 2A (49).

## 2.1.b Somatic uniparental disomy

Virtually, every cell line may be involved in clonal phenomena leading to UPD. However, this event is more frequent in cell populations characterized by a high turnover, such as hematopoietic and skin tissues. Indeed, acquired UPD seems to be due to errors happening during mitosis: the higher the rate of cell proliferation, the higher the risk of these errors occurring.

In most cases, acquired UPD is due to mitotic recombination between homologous chromosomes (Figure 2).

Figure 2- Mechanism of somatic uniparental disomy formation: "A" chromosome is used as template for reparation of its homologue "B" chromosome if a stochastic damage occurs during DNA replication
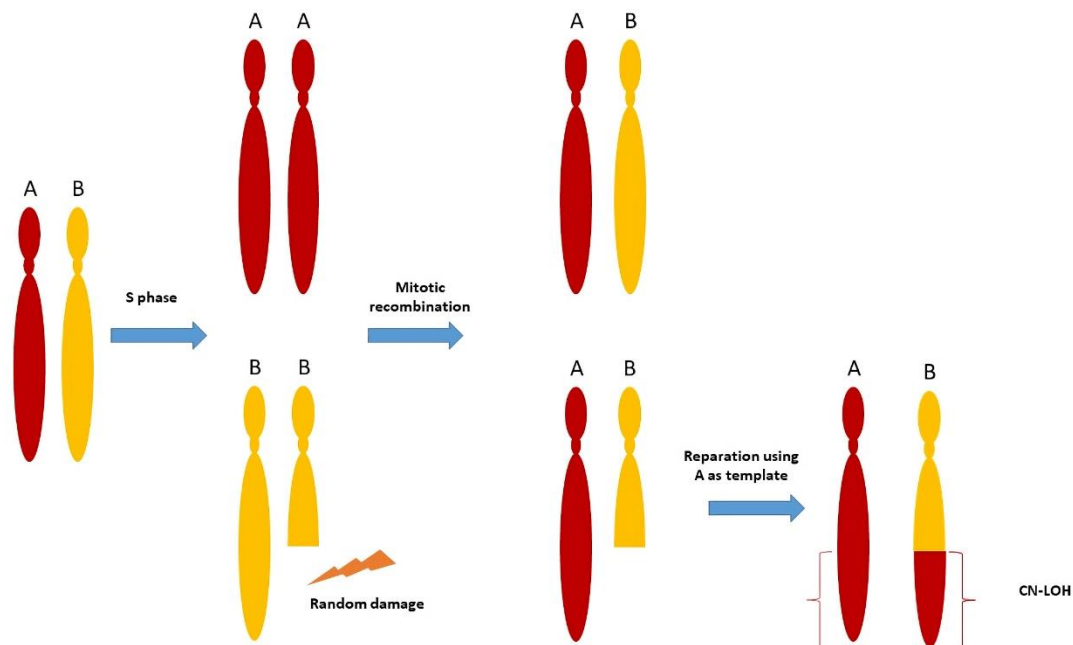
This phenomenon plays a critical role in repairing random errors happening during DNA replication. In particular, it occurs before cell enters mitosis, shortly after DNA replication, in the S phase, taking advantage of the accessibility of sister chromatids. Indeed, they represent the ideal template for reconstructing DNA that has been lost or damaged. Several mechanisms are involved in re-activation of replication from sister chromatids (50). Most of them are unknown but ongoing studies on unicellular eukaryotic organisms are helping to elucidate them: as soon as DNA damage is detected, the protein poly [ADP-ribose] polymerase 1 (PARP-1) is recruited to break-down the chromatin, via ADP-rybosilation of histones. Few seconds later, double-strand break repair protein MRE11 induces a rupture in the relaxed DNA exactly at the point where replication should begin (51). As such, at the end of reparative replication, two genomic portions that are equal to each other are generated, with subsequent loss of heterozygosity.

In a tumor population, dysregulation of cell proliferation control mechanisms implies that there is an elevated rate of mitotic recombination compared with the normal cell population. Many genes involved in both hematologic and non-hematologic malignancies have been associated to the occurrence of neoplastic clonal UPD.

2.1.b.i Somatic uniparental disomy in solid malignancies

The role of UPD as co-responsible for tumorigenesis was first described in the context of retinoblastoma. This is the most frequent tumor of pediatric age, due to mutation of tumor-suppressor gene *RB1* on chromosome 13q14.2. In 1983, Knudson showed through statistical analysis that the monoallelic aberration can be either congenital or acquired (52). However, the pathologic phenotype only arises if both alleles are involved, due to mitotic recombination with loss of the wild-type gene. The gradual refinement of diagnostic techniques allowed a better dissection of this phenomenon in many other malignancies. Due to its high frequency, many studies were performed on breast cancer and led to identification of high rate of CN-LOH in chromosomes 17p13.1 and 9p21.3, harbouring *TP53* and *CDKN2A/B* respectively (53, 54). Despite that, no clear correlation was proven to exist between these lesions and the outcome. In contrast, the CN-LOH pattern allowed a clustering of a series of lung cancers according to histologic type and, subsequently, prognosis (55). Later, a recurrent association between presence of CN-LOH and mutations in key-genes with adverse impact on prognosis was described in many other cases. In patients with basal cell carcinoma, the alteration of the tumor-suppressor *PTCH* was related to UPD in the region 9q21-q31 (56). A strong correlation between an overall high amount of CN-LOH and mutated *BRCA1* and *BRCA2* emerged from a retrospective investigation on samples from high-grade ovarian cancer (57). A frequent phenomenon of mitotic recombination was also described next to *APC* locus on chromosome 5q21 in patients with early-stage colorectal cancer and linked to increased risk of evolution into a more aggressive disease (58).

## 2.1.b.ii Somatic uniparental disomy in hematologic malignancies

In the hematologic field, the identification of CN-LOH as a potential tumorigenic mechanism is more recent. It is strictly associated to the introduction of cytogenetic diagnostic techniques based on dosage of allelic load [e.g. SNP-arrays, see 2.2]. These were first described in adult myeloid malignancies, in particular in myeloproliferative neoplasms (MPNs) with and without Ph chromosome, myelodysplastic syndromes (MDS) and acute myeloid leukemia (AML) (59). In all these cases, SNP-array analysis showed that CN-LOH are no randomly distributed across the genome with some chromosomes and chromosomal regions being more frequently affected, such as 7q, 9p, 13q and 17p. Molecular biology assays later proved that these alterations are commonly due to mutations in genes responsible for the control of cell proliferation, like *JAK2*, *TET2* and *CBL* (60). A modest incidence of CN-LOH was also confirmed in pediatric myeloid malignancies. In particular, a study showed UPD in 44% of pediatric patients with AML or MDS with an adverse impact on progression-free survival (PFS) only for those harbouring terminal CN-LOH>10 Mb (61). Following the characterization of CN-LOH in myeloid malignancies, some attempts were also made to define their potential role in the evolution of lymphoid neoplasms. In patients affected by multiple myeloma, aberrant plasma cells are enriched with UPD affecting chromosomes X, 1p, 6q, 8p, 13, 14q, 16q12-q23, and 17. Even if no evaluation of their influence on prognosis has been made until now, they are thought to have the same consequences of a loss (62). In mantle-cell lymphoma, the integration of SNP-array analysis with genome sequencing allowed the identification of recurrent CN-LOH in association with mutations affecting *TP53* and *CCDN1* genes (63).

## 2.1.b.iii Somatic uniparental disomy in B-cell acute lymphoblastic leukemia

First studies about CN-LOH in B-ALL were performed on pediatric patients, due to the high incidence of this disease in children compared to adults. In 2007, the presence of UPD along the genome of pediatric B-ALL patients was first proved by Mullighan et al. integrating data from both SNP-array analysis and whole genome sequencing (64). The following year, an international cooperative group evaluated by SNP-array CNVs on samples from 399 pediatric patients at baseline (65). UPD were detected in 24% of cases and confirmed as somatic on matched marrow cells after the achievement of a remission. The involvement of entire chromosomes prevailed in the hyperdiploid forms while the other subtypes were associated with CN-LOH spanning smaller regions, suggesting different mechanisms underlying the formation of these aberrations. The most frequent involved region was 9p without any evidence of mutations in the known genes mapping in this region. This data was later confirmed by cytogenomic analysis performed on 200 pediatric ALL (66). Even if CN-LOH in 9p were detected in 8% of patients, no case was associated with aberrations mapping in *CDKN2A/B* locus. Therefore, the involvement of other unknown genes should be postulated in the formation

of 9p UPD. 1p31.1, 10p11.2-10q11.21, 19p13.2-3 and 20q11.1-23 resulted enriched by CN-LOH in a following series of B-ALL pediatric cases (67). The few studies aimed to dissect the phenomenon of UPD in adult B-ALL showed pattern and frequencies comparable to those of the pediatric population. In particular, 9p resulted the most involved region in a Swedish series, followed by chromosomes 3, 5, 6q, 9q and 14q (68). In contrast to what was observed in the pediatric age, a statistically significant association of CN-LOH in 9p with homozygous loss of *CDKN2A/B* was demonstrated in these cases. More recently, the recurrence of CN-LOH affecting 12q also emerged in the adult B-ALL and was mainly associated to iAMP21 (69). The reasons for this association are unknown but *in vitro* studies showed that iAMP21 leads to over-expression of *DYRK1A*. This kinase cooperates with the hematopoietic regulator *SH2B3* on 12q24.12, found to be mutated in all cases harbouring UPD in 12q. A high incidence of UPD was also detected in a Russian cohort: 29/36 patients had CN-LOH along the genome, with those mapping in 10q and 11p strongly associated to MRD positivity. In contrast, the CN-LOH in 5q were exclusively found in MRD- cases (70). In conclusion, CN-LOH seem to occur also in the adult B-ALL with a non-negligible incidence. However, whether they affect or not the prognosis is still far to be fully elucidated.

2.2 Tools for detection of uniparental disomy

Along the years, different tools have been implemented in order to ensure a proper detection of CN-LOH in tumor samples.

Among these, the most standardized techniques are:

- SNP-array;
- Microsatellite analysis;
- Restriction Fragment Length Polymorphisms (RFLP) analysis.

SNP-array: it is a DNA array enriched with both CN and SNP probes. CN probes bind to highly conserved chromosomal regions and are required to have high specificity and sensitivity. The elevated specificity is needed to ensure exclusive recognition of a genomic region, avoiding overlapping with other similar areas. On the other hand, the high sensitivity is necessary to detect minimal variations of CN, allowing their identification also in tumor samples with aberrations in mosaicism. SNP probes are capable of detecting the 2 SN variants of a DNA sequence, reported as the 2 most frequent alleles in the general population and defined as *A* and *B*. This design grants the identification of either homozygosity or heterozygosity at each DNA region. Each of these probes is labelled with a fluorescent dye. Therefore, following hybridization of the array with the tumor sample, the release of a light signal of varying intensity according to the type of sequence occurs. In particular, if the sample is homozygous for an allele (*AA* or *BB*), it will only bind to the allele *A* or allele *B* position on the array, with emission of a very intense sign from only one of the two positions. In case of heterozygosity (*AB*), the sample will hybridize with both positions, releasing a double fluorescence with reduced intensity. Based on these principles, the entity of fluorescence will increase or decrease in presence of gains or losses, respectively. The resultant intensities are compared with normal control samples that are run independently and combined to create a reference data set. The following ratio between the test and the reference is converted to a CNV measurement. These values are imaged through dedicated software in the form of specific graphs, the "allele peaks" and the "smooth signal" charts. "Allele peaks" graphs allow the visualization of the signal intensity caused by the hybridization of sample with both specific alleles for each SNP. Under normal conditions, the signals are organized into three clusters corresponding to the three possible genotypes: *AA*, *BB*, *AB*. The "smooth signal" graph shows the mean signal intensity along the whole genome, via normalization methods that reduce background noise and highlight general trends in copy number. In the absence of alterations, we expect to visualize a "smooth signal" of two, corresponding to a diploid status. Therefore, the condition of CN-LOH is identified by the presence of only the two clusters *AA* and *BB* in the "allele peaks" graph and by the persistence of a "smooth signal" of two (71). CN-LOH detected by SNP-array are usually referred as regions of homozygosity (ROHs) (Figure 3).

Figure 3- Visualization of acquired regions of homozygosity by SNP-array: diploid state (CN2) is usually associated to three allele peaks (1+1), corresponding to AA, AB and BB combinations. In the presence of homozygosity, CN2 is associated to only two allele peaks (2+0), corresponding to AA and BB combinations.
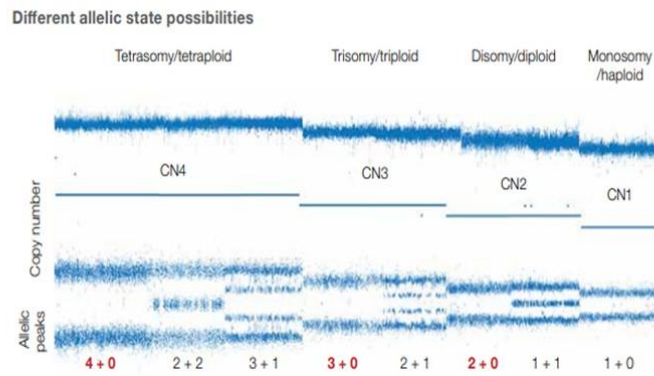


Figure modified from Thermofisher Scientific. Cytoscan comprehensive brochure. 2019.

Microsatellite analysis: microsatellites are short tandem repeats (STRs) of DNA consisting of 2-6 nucleotides and arranged throughout the whole genome. Since they are highly polymorphic even within the same population, STRs can be used for the identification of CN-LOH. Indeed, the genome of a healthy tissue and of a tumour tissue from the same person may be compared based on number of STRs: DNA from the 2 samples is amplified by PCR with specific primers for microsatellites and the products are separated by electrophoresis. In case of UPD affecting a genomic region in the tumor tissue, there will be a reduction in the number or size of bands at that region (72).

Restriction fragment length polymorphisms (RFLP) analysis: it is based on the possibility of fragmenting the genome using restriction enzymes. These proteins cut at sequences in positions varying from person to person. Therefore, using restriction enzymes on samples from a same person, fragments of different lengths will be generated in the presence of UPD (73).

Briefly, microsatellite and RFLP are simple and cost-effective techniques, while SNP array could be challenging and expensive. However, the first 2 techniques are burdened by a lower resolution since they only allow identification of CN-LOH affecting specific genomic regions; on the other hand, SNP analysis provides coverage of the entire genome, facilitating identification of UPD even in previously unexplored regions. The sensitivity of this technique is 20%, meaning that all the alterations with a variant allele frequency (VAF) ≥20% could be detected. Since B-ALL is defined by a BM infiltration≥20%, SNP-array analysis could be considered the most robust tool for UPD detection in this patients' setting (74).

More recently, the arsenal available for the characterization of UPD in hematologic patients has been enriched with the optical genome mapping (OGM), a novel high-resolution genome-wide technology revealing both structural (SVs) and copy-number variations (CNVs) in a single assay (see 8.2, 8.3).

We currently face the absence of consensus about the criteria to be adopted to study UPD when analysing a SNP-array. Based on the last guidelines published in 2016, the only CN-LOH to be reported are those independent from allelic imbalance (i.e. CNVs), larger than 10 Mb and extending to the chromosome telomeres (75). However, no size limitation for reporting of UPD is required if the call is reliable and made with a sufficient number of probes. The absence of limits in size and location of CN-LOH was also confirmed by the consensus recommendations from the American college of cytogenetics (76). According to this position paper, we should report all regions of UPD including oncogenes and/or tumor-suppressor genes since they may have a clinical value. These recommendations also underline the need to specify whether the aberration is somatic or germinal. The identification of the UPD origin may be challenging. The best technique to define this is to study 2 samples in parallel:

-the sample from the tissue infiltrated by the tumor at baseline *vs* the sample from the same tissue after the remission defined with high-sensitive tools;

-the sample from the tissue infiltrated by the tumor at baseline *vs* the sample from any uninfiltrated tissue (e.g. fibroblasts, scalp or oral mucosa).

When the healthy control is not available, the use of VAF determination is strongly recommended. A germinal origin should be suspected in the case of 100% cell involvement or of any percentage higher than that corresponding to tumor infiltration.

## 3. Aim of the study

UPD plays a role in tumorigenesis. The introduction into the cytogenetic work-up of techniques based on measurement of allelic load has allowed identifying the recurrence of this phenomenon also within the hematologic malignancies. However, to date, few studies have investigated the prognostic value of CN-LOH in adult B-ALL. The paucity of data may be due both to the relative rarity of this disease and to the absence of consensus about the criteria to be adopted to study UPD when analysing a SNP-array (see above).

Thus, the evaluation of CN-LOH in the current cytogenetic work-up of adult B-ALL still represents an "unmet laboratory need". To date, the adult population suffers from a dismal prognosis compared to the pediatric counterpart, in spite of the refinement of treatment backbone. Therefore, a deeper understanding of all biological mechanisms underlying leukemogenesis, including UPD, could help refine the cytogenetic risk-stratification, resulting in the possibility of improving and personalizing therapy. In the present study, we retrospectively analyzed the CN-LOH detected by SNP-array in a longitudinal cohort of adult B-ALL patients and aimed to dissect any possible correlation with both clinical and biologic data and with prognosis.

## 4. Materials and methods

The study was carried out at the Cytogenetic Unit of the Catalan Institute of Oncology-Josep Carreras Leukemia Research Institute (Badalona, ES). Patients with B-ALL enrolled in the clinical trial NCT04179929 (LAL-19) with available SNP-array analysis performed at baseline for genetic risk-stratification as per protocol were considered evaluable.

LAL-19 is an ongoing Spanish interventional multicentre clinical trial enrolling patients aged 18-60 years affected by Ph- T and B-ALL. The aim of the study is to provide a common treatment for adult patients, with improvement of overall survival (OS). This goal is pursued by stratifying the treatment according to MRD evaluated at certain time-points during the treatment and the genetic features identified at baseline by molecular biology and a cytogenetic work-up, including chromosomal-banding analysis (CBA), FISH analysis if indicated, SNP-array analysis and NGS with specific panels.

For B-ALL, the high-risk genetic aberrations are defined as follows:

- Hypodiploidy (i.e. <40 chromosomes in patients older than 35 years);
- *KMT2A* rearrangements;
- *TP53* homozygous deletion and/or mutation;
- Concomitant deletion of *IKZF1* and *CDKN2A/B* (*IKZF1*$^{plus}$ signature).

For T-ALL, the unfavourable profile is represented by unmutated *NOTCH1/FBXW7* and/or mutations affecting *RAS/PTEN*.

According to the protocol, all patients are uniformly treated with a first four-drug induction, followed by a second intensive induction (or immunotherapy with inotuzumab ozogamicin) in case of resistance and by early consolidation if an adequate MRD clearance is achieved at the end of induction. After consolidation, patients with adequate MRD clearance and absence of high-risk genetic features will proceed to intensification, re-induction and maintenance with only chemotherapy while the other patients will undergo allogenic stem-cell transplant (HSCT). Early T-cell precursor ALL cases follow a differentiated treatment and all undergo HSCT a priori.

SNP-array analysis was performed on genomic DNA extracted by any commercial kit from BM samples only if a blastic infiltration of at least 20% was reported. The Affymetrix Cytoscan Assay protocol (Santa Clara, CA, US) was used.

This protocol consisted of 4 days. During the first day, genomic DNA underwent digestion with nuclease and ligation with PCR-adapter. The following day, a standard PCR was performed and the quality of amplicon was evaluated by quality-control (QC) electrophoresis with 2% agarose gel. After purification of PCR products, an aliquot was used for quantitation by nanodrop. An amount of genomic DNA ranging between 40 and 70 ng/µl

was considered suitable for the following steps. On the third day, amplicon underwent mechanic fragmentation, and then another QC electrophoresis with 3% agarose gel was performed. If all the parameters were within the range, labelling was carried out using terminal deoxynucleotidyl transferase for incorporation of biotin-labelled nucleotides and then we proceeded with loading of labelled DNA into the specific array (Affymetrix GeneChip Mapping 750 K array). After overnight hybridization, several washing steps were performed to remove any un-hybridized residue. Therefore, staining with streptavidin-peroxidase was performed and the array was loaded onto the GeneChip Scanner. In order to assess the good quality of the entire process, 3 main parameters were taken into account:

- Median Absolute Pairwise Difference (MAPD): it assesses signal intensity variability between adjacent probes. Indeed, these probes should emit signals with similar intensity;
- Single Nucleotide Polymorphism Quality Control (SNPQC): it assesses the reliability of calls at the level of each SNP probe, based on the separation between clusters of homozygous and heterozygous genotypes;
- Waviness: it measures the long-range oscillation of signal intensity along the genome, allowing for identification of background noise.

Analysis of the data from the array of each sample was considered possible if the parameters were as follows:

-MAPD ≤ 0.25;

-SNPQC ≥ 15;

-Waviness ≤ 0.12.

The results were scored using CHAS v4.5 software (Affymetrix). The condition of CN-LOH was defined by the presence of only the two clusters *AA* and *BB* in the "allele peaks" graph and by the persistence of a "smooth signal" of two, as commented above. For the aim of the study, we first selected ROHs with size≥3 Mb and mapping in regions covered with≥20 consecutive probes. In order to identify only acquired non-polymorphic forms (aROHs), we excluded ROHs overlapping ≥50% of their length with regions included in public databases of healthy controls and with VAF>BM infiltration. Finally, eligible calls were cross-referenced with patients' biological and clinical data for statistical analysis.

For conventional statistical analysis, continuous variables were expressed as median and categorical variables as percentage frequencies. Differences between categorical variables in the analyzed population were assessed by Chi-Square test or Fisher's exact test; Mann-Whitney test was used for comparison between continuous variables. OS was defined as the time interval expressed in months from the date of treatment initiation to the date of last follow-up or the date of death. Analysis of OS was performed by Kaplan-Meier (KM) curves, and differences between KM curves were assessed by the log-rank test. Cumulative incidence

of relapse (CIR) was calculated as the time interval in months from the date of complete remission to the date of disease progression and was estimated using cumulative incidence functions by competing risks analysis (being death in remission the competitor). Gray's test was used for comparison of CIR curves. Statistical significance was considered for values of $p < 0.05$. All analyses were performed using SPSS (v.24) and R (v.3.5.2) software. The results of the standard statistical analysis are currently undergoing validation by artificial intelligence techniques. Specifically, for the aim of the study, two models are being employed:

-light Gradient Boosting Machine (lightGBM): a gradient boosting algorithm based on decision trees;

-sequential neural network in Keras (NN): a linear algorithm based on progressive stacking of layers of data.

Each model will be trained through fine-tuning processes to increase the accuracy of the predictions.

## 5. Results

### 5.1.a General features of the whole population

From December 2019 to March 2024, 371 B-ALL patient were included in the LAL-19 clinical trial. Evaluation of ROHs along the genome by SNP-array analysis was possible in 277 cases (75%). The remaining cases were not evaluated due to lack of available material.

Overall, the median age of study cohort was 40 (range 18-60 years old), with 51% of patients being classified as adolescents-young adults (AYA). The male-female ratio was 1:1. The B-common phenotype was detected in 77.3% of cases, followed by the pro-B and the pre-B, being detected in 17.3% and 5.4% of patients, respectively. The median white blood cell (WBC) count at onset was $12.80x10^9$/L (0.60-720). Twenty-four cases (13.5%) had hyperleukocytosis, defined by WBC count≥$30x10^9$/L. The assessment of central nervous system involvement was possible in 176 patients and was positive in 24 cases (13.6%).

For each patient, CBA was locally performed on unstimulated 24-hour culture PB or BM samples. The study was considered evaluable if at least 20 metaphases in absence of any alteration or 10 metaphases in presence of any alteration were evaluable (77). The results were reported according to International System for Human Cytogenetic Nomenclature (ISCN 2020). At data cut-off, karyotype description was available in 204 cases. The absence of metaphases was observed in 46 patients (22.5%). Sixteen cases (7.8%) had normal karyotype; among the remaining patients with altered CBA, a great variety of aberrations was described, with *KMT2A* rearrangements being the most recurrent (31 cases). A complex karyotype, defined by ≥5 aberrations, was reported in 25 cases (12%).

FISH analysis was performed according to local policies based on karyotype results. At data cut-off, it was available for 245 patients with break-apart probes for *CRLF2* being the most used one. It proved a rearrangement in 21 cases (8.5%).

229 patients also had NGS analysis done through in-house panels specifically designed for the detection of B-ALL mutations. The most frequent aberrations where those affecting RAS-pathway, detected in 95 cases (41.5%).

SNP-array analysis was centralized. It proved the presence of CNVs in 261 pts (94%). In particular, this tool enabled the detection of *IKZF1^plus* profile in 66 cases (25%).

Overall, 95 out of 268 patients (35.4%) evaluable for risk stratification, as per protocol, belonged to the high-risk category. Stratifying patients according to WHO 2022 and according to ICC 2022, the NOS category was the most represented (42.5% of cases), followed by Ph-like and *KMT2A* rearrangements groups, including 11.7% and 11.3% of patients, respectively (Table 2).

Table 2- Clinical features of the study cohort

| | | Whole cohort (N=277) | | Cohort with aROHs (N=156) | | Cohort without aROHs (N=121) | |
|---|---|---|---|---|---|---|---|
| **Median age [range]** | | 40 [18 – 60] | | 39 [18 – 60] | | 41 [18 – 60] | |
| **Gender** | Male | 137/262 | (52.3%) | 75/145 | (51.7%) | 62/117 | (53%) |
| | Female | 125/262 | (47.7%) | 70/145 | (48.3%) | 55/117 | (47%) |
| **WBC count** | < 30x10$^9$/L | 153/177 | (86.5%) | 78/87 | (90%) | 75/90 | (83%) |
| | > 30x10$^9$/L | 24/177 | (13.5%) | 9/87 | (10%) | 15/90 | (17%) |
| **CNS involvement** | Yes | 24/176 | (13.6%) | 12/90 | (13.3%) | 12/86 | (14%) |
| | No | 152/176 | (86.4%) | 78/90 | (86.7%) | 74/86 | (86%) |
| **Genetic subtype according to ICC and WHO 2022** | NOS | 116/273 | (42.5%) | 74/156 | (47.4%) | 42/117 | (36%) |
| | Ph-like | 32/273 | (11.7%) | 19/156 | (12.1%) | 13/117 | (11.1%) |
| | *KMT2A*-r | 31/273 | (11.3%) | 17/156 | (10.9%) | 14/117 | (12%) |
| | Hypodiploidy | 24/173 | (8.8%) | 7/156 | (4.5%) | 17/117 | (14.5%) |
| | PAX5-m | 21/273 | (7.7%) | 13/156 | (8.4%) | 8/117 | (6.8%) |
| | t(1;19) | 17/273 | (6.3%) | 10/156 | (6.4%) | 7/117 | (6%) |
| | Hyperdiploidy | 15/273 | (5.4%) | 9/156 | (5.8%) | 6/117 | (5.1%) |
| | Others | 17/273 | (6.3%) | 7/156 | (4.5%) | 10/117 | (8.5%) |
| **Genetic classification according to PETHEMA LAL-19** | Standard risk | 173/268 | (64.6%) | 101/151 | (66.9%) | 72/117 | (61.5%) |
| | High risk | 95/268 | (35.4%) | 50/151 | (33.1%) | 45/117 | (38.5%) |

Abbreviations:

aROHs= acquired regions of homozyogosity; WBC= white blood cells; CNS= central nervous system;

-r= rearrangement; -m= mutation.

"Others" include cases with n<10

[*ZNF384*-r= 5, iAMP21=4, t(12;21)= 2, *MYC*-r=2, *MEF2D*-r=1, other recurrent aberrations= 3]
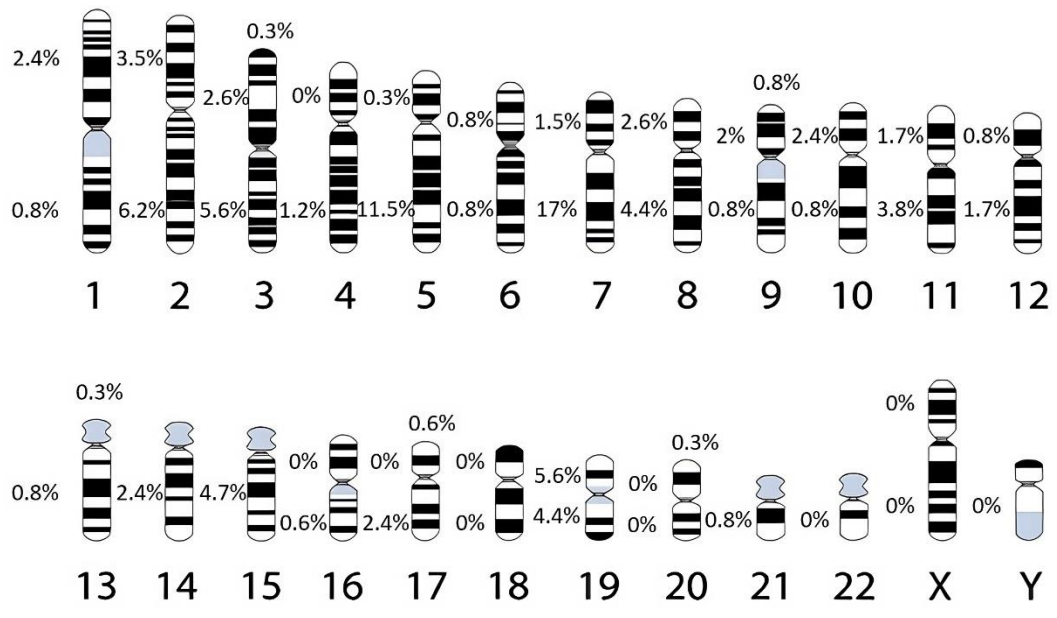
5.1.b Distribution of acquired regions of homozygosity

Overall, 339 aROHs were detected in 156 patients (56%). The median number of aROHs per patients was one (range 1-9); the median size was 6.7 Mb (range 3-27.5). The global extent of these alterations was shorter than 10 Mb in most cases (109 patients, 69.9%). Twenty cases (12.8%) showed involvement between 10 and 20 Mb, and 27 cases (17.3%) had involvement larger than 20 Mb. Ninety-four % of aROHs were segmental (interstitial calls=278; telomeric calls=41). The involvement of whole arms or entire chromosomes was recorded only in 12 and 8 cases, respectively. aROHs were unevenly distributed across the whole genome. In particular, chromosomes 7, 5 and 19 were the most affected, harbouring 16%, 11% and 10% of all calls, respectively. On the other side, no aRHOs were detected in chromosomes 18, 22, X and Y (Table 3, Figure 4).

Table 3- Features of acquired regions of homozygosity

| Total number of aROHs calls | | 339 | |
|---|---|---|---|
| **Position of aROHs along the chromosome** | Interstitial | 278 (82%) | |
| | Terminal | 41 (12.2%) | |
| | Whole arm | 12 (3.5%) | |
| | Whole chromosome | 8 (2.3%) | |
| **Median number of aROHs per patient [range]** | 1 [1-9] | Number of aROHs/pt | Number of pts (N=156) |
| | | 1 | 80 (51.4%) |
| | | 2 | 45 (28.8%) |
| | | >2 | 31 (19.8%) |
| **Median size of aROHs [range]** | 6.7 Mb [3-27.5] | Global extent of aROHs/pt | Number of pts (N=156) |
| | | <10 Mb | 109 (69.9%) |
| | | >10/<20 Mb | 20 (12.8%) |
| | | >10 Mb | 27 (17.3%) |

Figure 4- Distribution of acquired regions of homozygosity along the genome of the study cohort



Legend:

The percentages of acquired regions of homozygosity (aROHs) detected for each chromosome are shown on the left, next to short and long arms according to their position. The percentages at the top for chromosomes 3, 9, 13, 17 and 20 correspond to aROHs involving the whole chromosome
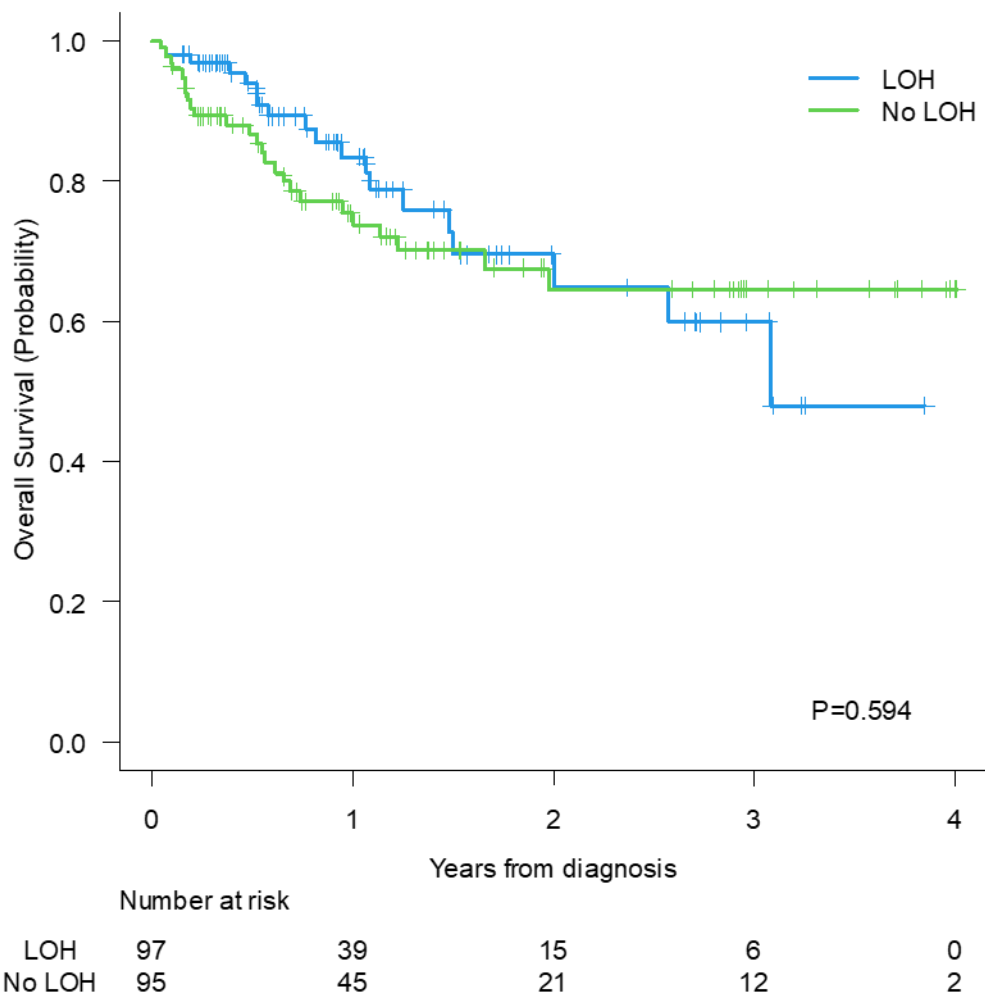
5.1.c Correlation between acquired regions of homozygosity and clinical features at onset

No difference was observed between patients with and without aROHs in terms of age, sex and clinical features at the onset. However, the presence of aROHs was associated with the absence of hypodiploidy (<44 chromosomes) and absence of mutations in the survival regulatory pathways detected by NGS standard panel (p=0.029 and p=0.043, respectively).

5.1.d Survival analysis

At data cut-off, survival analysis was possible in 192 patients (69%). After a median follow-up of 1 year (range 01.0-4), the presence of aROHs had no impact on either OS (p=0.594) or CIR (p=0.893) (Figures 5). Within the population with aROHs, no difference emerged in terms of OS and CIR stratifying by number (1 *versus* >1) and size of lesions (<20 Mb *versus* >20 Mb, being 20 Mb the most employed cut-off in literature) (Figures 6).

Figure 5.a. Comparison between overall survivals of patients with and without acquired regions of homozygosity



| | LOH<br>(n=97) | No LOH<br>(n=95) |
|---|---|---|
| 2-year OS (95%CI) | 70% (54% - 81%) | 65% (51% - 75%) |
| 3-year OS (95%CI) | 60% (41% - 75%) | 65% (51% - 75%) |

Figure 5.b. Comparison between cumulative incidences of relapse of patients with and without acquired regions of homozygosity
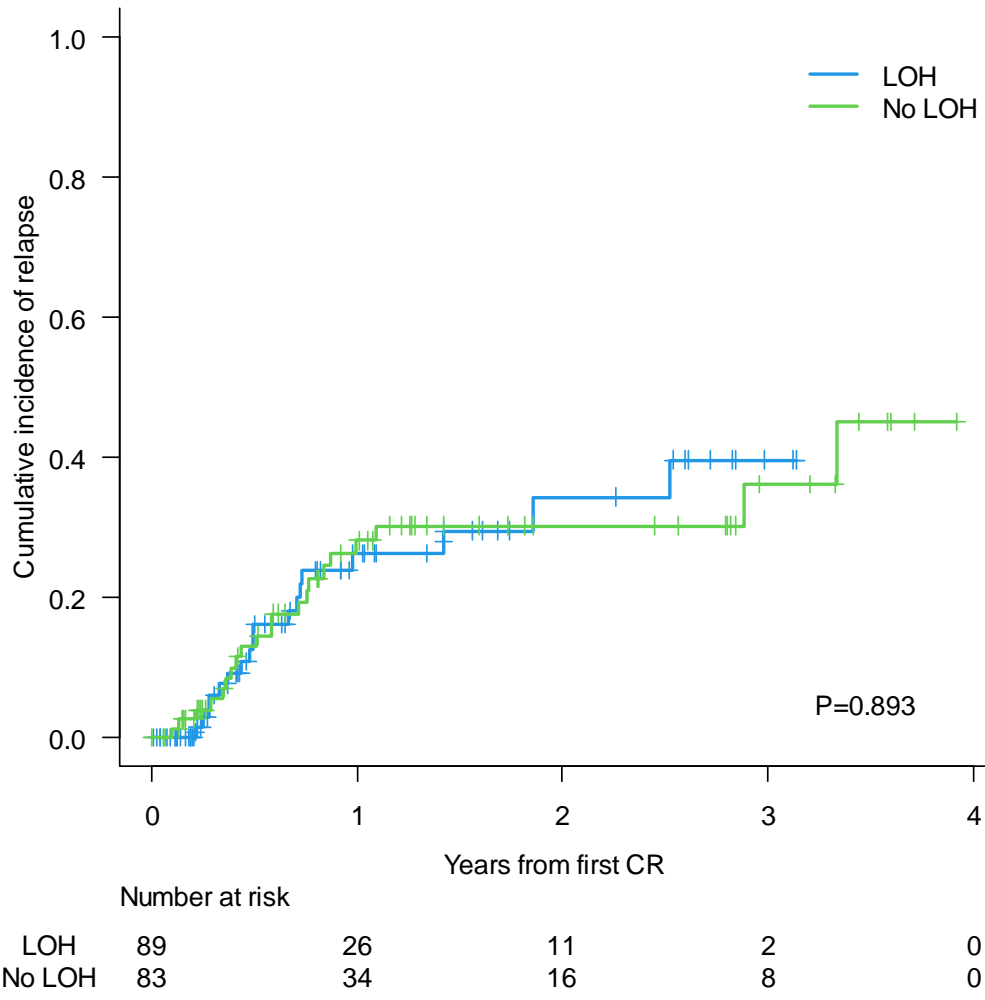


| | LOH (n=89) | No LOH (n=83) |
|---|---|---|
| **2-year CIR (95%CI)** | 34% (20% - 49%) | 30% (19% - 42%) |
| **3-year CIR (95%CI)** | 40% (22% - 56%) | 36% (21% - 52%) |

Figure 6.a. Comparison between overall survivals of patients with acquired regions of homozygosity stratified according to the number of calls detected along the whole genome
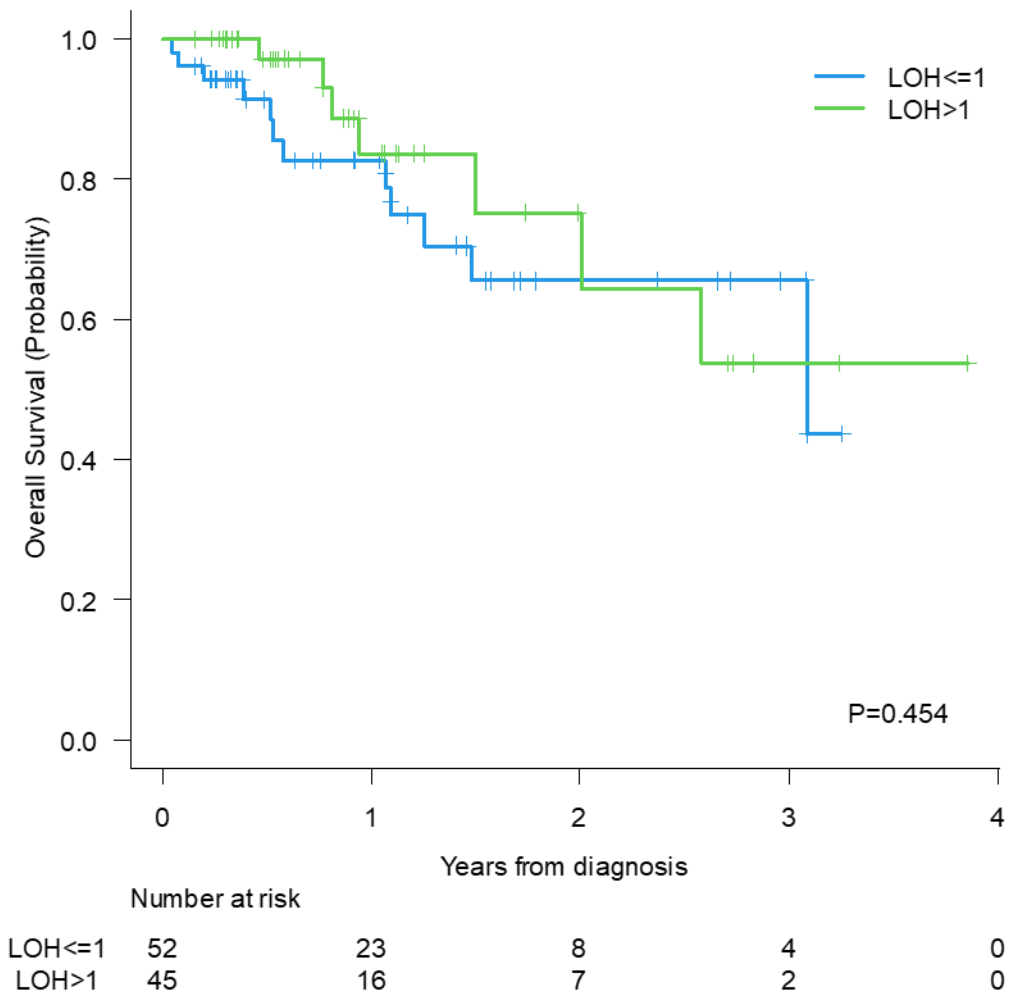


| | LOH ≤1<br>(n=52) | LOH >1<br>(n=45) |
|---|---|---|
| 2-year OS (95%CI) | 65% (45% - 80%) | 75% (47% - 90%) |
| 3-year OS (95%CI) | 65% (45% - 80%) | 54% (23% - 77%) |

Figure 6.b. Comparison between overall survivals of patients with acquired regions of homozygosity stratified according to their size
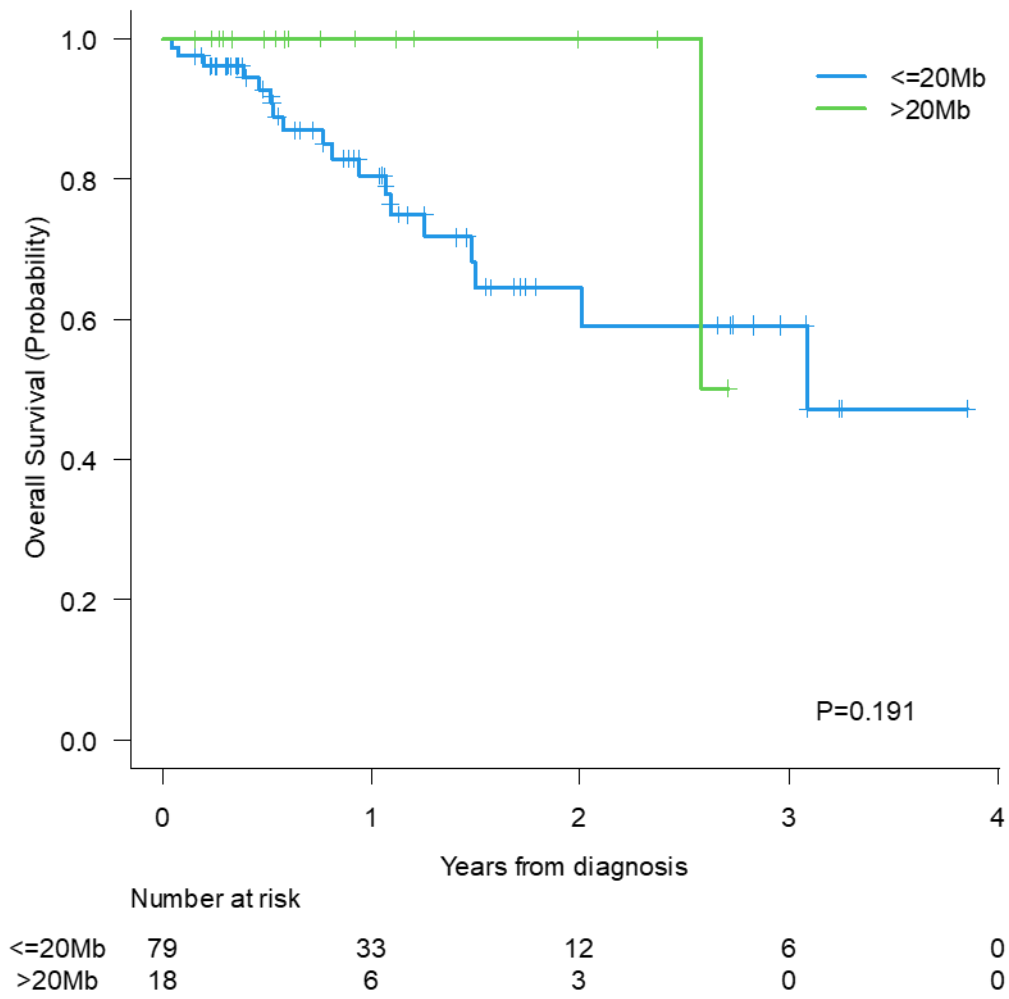


| | Tamaño LOH ≤20 (n=79) | Tamaño LOH >20 (n=18) |
|---|---|---|
| **2-year OS (95%CI)** | 65% (47% - 78%) | 100% |
| **3-year OS (95%CI)** | 59% (40% - 74%) | No hay suficiente seguimiento |

Figure 6.c. Comparison between cumulative incidences of relapse of patients with acquired regions of homozygosity stratified according to the number of calls detected along the whole genome



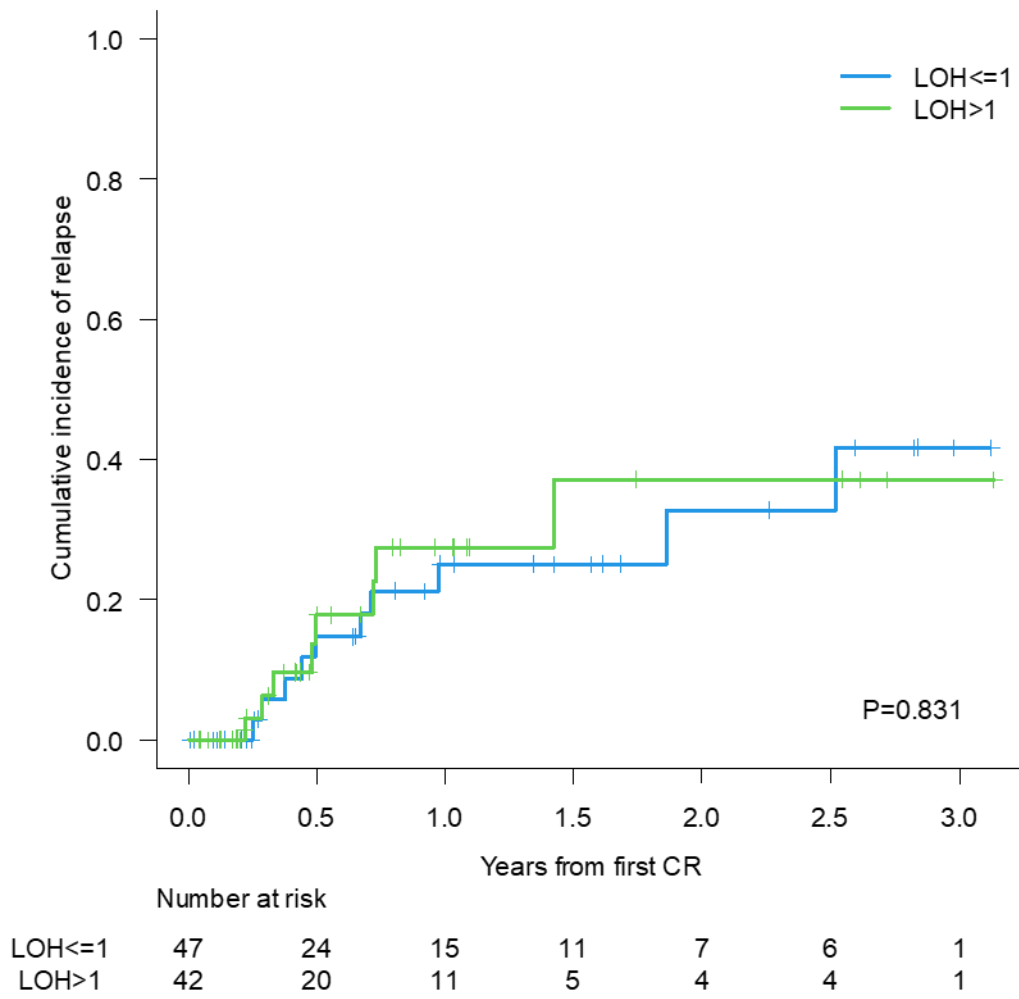| | LOH ≤1 (n=47) | LOH >1 (n=42) |
|---|---|---|
| **2-year CIR (95%CI)** | 33% (14% - 53%) | 37% (14% - 61%) |
| **3-year CIR (95%CI)** | 42% (18% - 64%) | 37% (14% - 61%) |

Figure 6.d. Comparison between cumulative incidences of relapse of patients with acquired regions of homozygosity stratified according to their size
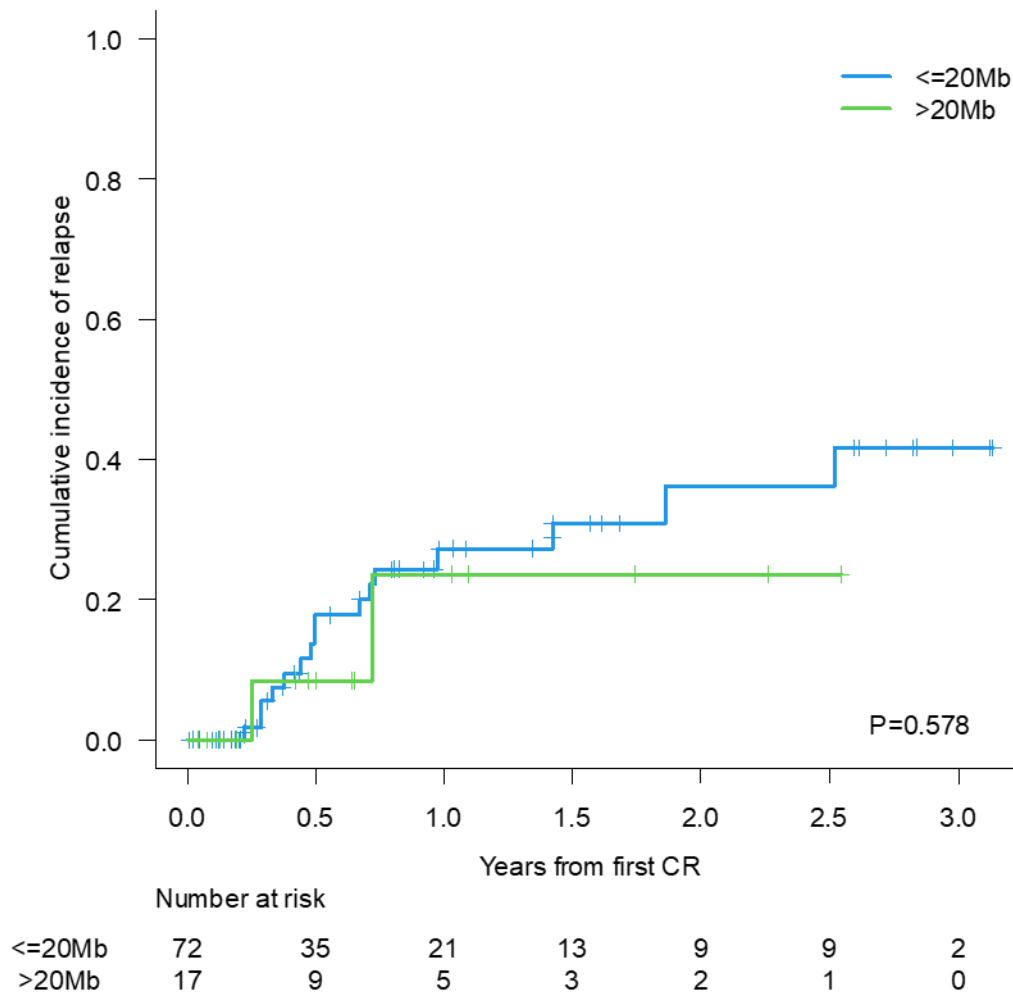


| | Tamaño LOH ≤20 (n=72) | Tamaño LOH >20 (n=17) |
|---|---|---|
| **2-year CIR (95%CI)** | 36% (20% - 53%) | 24% (2% - 58%) |
| **3-year CIR (95%CI)** | 42% (23% - 59%) | No hay suficiente seguimiento |

## 6. Discussion

This study shows that the genome of adult patients affected by B-ALL is enriched with aROHs. Indeed, these alterations were detected in more than half of the large study cohort, which was homogeneous with regard to demographic and clinical characteristics. This finding is consistent with the limited available literature. However, a direct comparison of the few works is not possible, since ROHs were not always identified only with SNP-array. Furthermore, within the studies using this latter technology, no common guidelines were employed. Most of the previous papers mentioned above included ROHs harbouring or adjacent to regions of CNVs. This criterion may have led to the identification of recurrent ROHs on 9p21.3, due to high frequency of deletions affecting genes in this region, such as *CDKN2A/B* (64, 68). Here, we excluded ROHs that partially or entirely overlapped with gains or losses since we assumed that in the presence of CNVs, the LOH call by SNP array was unreliable due to the signal disruption. Therefore, in our study, 9p21.3 was affected only in 2.8% of cases while the most frequently involved regions were 5q31.1 and 7q11.23, harbouring 17% and 11.5% of all calls, respectively. Both regions are loci of numerous coding and non-coding genes but only few of them overlapped with B-ALL BED files we used for SNP-array analysis. In particular, 5q31.1 includes *AFF4*, *IL3*, *FNIP1*, *IRF1* and 7q11.23 contains *BCL7B*, *HIP1*, *CLDN4*, *HSPB1*, *LIMK1*. To the best of our knowledge, none of these genes plays a central role in B-leukemogenesis and only some anecdotal cases pointed out their marginal involvement in the disease. In our study, the recurrence of aROHs in regions devoid of driver genes could explain the absence of impact on prognosis. This neutral effect could be explained by distinguishing UPD harbouring or not mutations of driver genes. Actually, these aberrations derive from 2 separate aetiologies and seem to appear in distinct moments of tumorigenesis. According to the literature, aROHs including mutated driver genes appear later than the mutation, as its consequence (78). Indeed, the same mutation ensures a proliferative advantage and, within the context of this selective pressure, the mitotic recombination acts to remove the wild-type allele (79). On the contrary, the mechanisms underlying aROHs affecting non-driver genes are more complicated and still poorly understood, based on the paucity of available data (80, 81). In most cases, they affect genomic areas which are responsible for the maintenance of cellular homeostasis, and seem to play an important role at the early stage of tumor development (82). Consequently, we could speculate about a possible protective role of the aROHs affecting non-driver genes identified across our whole cohort. Indeed, no statistically significant difference was observed between patients with and without aROHs and, within the aROHs cohort, the group with a genomic involvement larger than 20 Mb had a survival benefit. However, this advantage was not statistically significant, probably due to the short follow-up. Furthermore, we also observed a negative correlation between their presence on the one hand and the presence of mutations detected by NGS and hypodiploidy on the other hand. Both latter phenomena are known to be adverse prognostic factors (83, 84) and does not seem to occur so early during

the tumor development (83). Therefore, aROHs of non-driver genes detected in our study along the genome of adult patients with B-ALL could represent an early phenomenon preventing from acquisition of aneuploidies and point mutations, reflecting more efficient machinery of DNA reparation compared with patients without aROHs.

7. Conclusion

Our study proves the recurrence of aROHs along the genome of B-ALL adult patients. These aberrations display an irregular distribution, with long arms of chromosomes 5 and 7 being the most affected regions. Most of aROHs do not involve driver genes for leukemogenesis. Therefore, they do not exert any impact on prognosis. On the contrary, aROHs could play a protective role for the genome, due to their association with a low rate of mutations and with preserved diploidy. This hypothesis is undergoing further evaluation using a machine learning approach.

**Project 2**- Unveiling the genetic landscape of B-cell precursor acute lymphoblastic leukemia by novel technologies: optical genome mapping versus digital multiplex ligation dependent-probe amplification

ABSTRACT

**INTRODUCTION**

Adult B-cell acute lymphoblastic leukemia (B-ALL) is a heterogeneous hematologic malignancy, characterized by progressive accumulation of several genomic lesions. About 10-30% of cases remain unclassifiable by routine cytogenetic tests (RT) (i.e. chromosomal banding analysis, fluorescence in situ hybridization, chromosomal microarrays). Therefore, novel technologies are required for a more extensive assessment of B-ALL genetic background, in order to improve risk-stratification and to personalize treatment. Optical genome mapping (OGM) is a high-resolution genome-wide tool revealing structural (SVs) and copy-number variations (CNVs) by fluorescent labelling and digital imaging of ultra-high molecular weight (UHMW) DNA molecules. Digital multiplex ligation dependent-probe amplification (dMLPA) combines standard MLPA with next generation sequencing for detection of CNVs and gene fusions due to interstitial deletions (dels).

**AIM**

The project aims to evaluate if OGM and dMLPA could integrate RT to improve the cytogenetic profiling of adult B-ALL.

**METHODS AND RESULTS**

For the purpose of the study, we selected a cohort of adult B-ALL patients (pts) with sufficient leftover material after RT at baseline. OGM was performed (in Spain) following manufacturer's instructions (BionanoGenomics, San Diego, US): UHMW-DNA was extracted, labelled with DLE-1 enzyme, loaded onto a chip and run by Saphyr instrument. Data analysis was carried out through rare variant analysis algorithm on BionanoSolve software, using GRCh37/h19 as genome reference. SVs and CNVs were considered if overlapping with regions included in open-access BED files for B-ALL or if ≥ 100 kb. The dMLPA experiments were performed (in Italy), in accordance with the manufacturer's instructions, using D007 ALL probemix (MRC Holland, Amsterdam, NL). The sample-specific products from several reactions were pooled and loaded on an Illumina MiSeq V3 flow-cell. The data were analyzed using bioinformatics software by MRC, Holland. Twenty cases were collected from May 2023 to July 2024. Median age was 50 years (range 18-70). The male/female ratio was 1:1. Based on RT, they were classified according to ICC 2022 as follows: NOS (not otherwise specified), 10 pts; Ph-like, 6 pts; *KMT2A*-rearranged (-r), 1 pt; *PBX1*-r, 1 pt; low-hypodiploidy, 1 pt; PAX5-mutated (-mut), 1 pt. OGM detected all previously known CNVs and SVs, except for two *CRLF2*-r. Furthermore, it detected driver SVs missed by RT with subsequent re-stratification of four cases: *ZNF384*-r in 2 NOS pts; *MEF2D*-r in 1 NOS pt and *EPOR*-r in PAX5-mut pt. dMLPA detected all CNVs and only SVs due to dels, included 1 *CRLF2*-r missed by OGM. Moreover, it detected with greater accuracy CNVs affecting genes with prognostic impact but no effect on classification (i.e. *EBF1*, *IKZF1*, *CDKN2A/B*, *PAX5*, *BTG1*, *TCF3* and *VPREB1*). Overall, the two techniques provided useful information for more accurate cytogenetic diagnosis and risk-stratification in 11 pts (55%).

**CONCLUSION**

To the best of our knowledge, this is the first study to integrate simultaneously OGM and dMLPA in the cytogenetic diagnosis of adult B-ALL. Both techniques outperformed RT for the detection of SVs and CNVs, respectively, showing high sensitivity and specificity, in accordance with the literature data. In particular, they proved useful for a more in-depth characterization of challenging categories, such as NOS and Ph-like. Greater experience is required to clarify the correct placement of OGM and dMLPA in the cytogenetic diagnostic algorithm of adult B-ALL.

8.1 Routine testing for cytogenetic diagnosis of B-cell precursor acute lymphoblastic leukemia

The current cytogenetic diagnosis of adult B-ALL is mostly based on CBA, integrated with FISH analysis and genomic microarray.

CBA: this technique is based on the possibility of producing a banding pattern on metaphases chromosomes, by exploiting the presence of both AT- and CG-rich areas. After a 24-hour sample culture, the cell life cycle is arrested by colchicine treatment. This is followed by treatment with hypotonic solution of 0.075 molar potassium chloride and multiple washing steps with Carnoy solution to isolate metaphases. The genetic material is then smear onto slides and, if chromosomes arrested in metaphases are present, specific staining for banding is performed. In most cases, Giemsa (G) stain is used: after G-banding, the chromosomes will appear characterized by alternation between dark and light bands. Dark bands correspond to AT-rich areas (i.e. heterochromatin), since these two nitrogen bases are only linked by two hydrogen bonds that are easy to break and let the colour penetrate. Light bands are located at the CG-areas (i.e. euchromatin), where G meets greater resistance. Quinacrine and reverse bandings are more rarely used methods. CBA provides a single cell whole genome view, allowing detection of structural and numerical CIN with a maximum resolution of 5 Mb.

FISH: this technique uses fluorophore-tagged probes which are perfectly complementary to a nucleotide sequence of interest. It can be performed either on metaphases or interphases nuclei. Therefore, the workflow includes slide preparation with aliquots of the sample and probe of choice, hybridization, washing steps to remove any un-hybridized residual and application of fluorescent stain DAPI to facilitate reading under a fluorescence microscope. FISH analysis enables detection of *a priori* suspected alterations with a range between 1 Mb and 50 Kb.

Genomic microarray: it is a collection of microscopic DNA spots attached to a solid surface. Different types are available but SNP-arrays are the most indicated for integrating the cytogenetic diagnosis of B-ALL (see 2.2), since they allow detection of any CNV larger than 20 Kb.

Even if the identification of most of the driver aberrations is possible by the integration of these techniques, some limitations should be taken into account. CBA depends on the growth of the cell clone and many environmental factors are involved. Furthermore, some aberrations do not involve the exchange between dark and light bands and are cryptic, e.g. some *KMT2A* rearrangements, t(12;21)(p13;q22). FISH analysis requires prior suspicion of the alterations and probes are not available for each of them. Genomic microarray misses all the structural CIN if there is no loss of material (e.g. balanced translocation). Therefore, as commented above, up to 30% of adult B-ALL cases remains unclassified by routine diagnostic testing (RT).

Novel tools are required for a more extensive evaluation of genetic landscape underlying B-ALL onset and, among these, OGM and digitalMLPA (dMLPA) could be ideal candidates.

8.2 Optical genome mapping

8.2.a General principles

This technique was first described by Schwartz in 1993 to study the genome of *Saccharomyces cerevisiae*: after extraction, large DNA molecules were digested by restriction enzymes, elongated by electrophoresis and imaged by fluorescence microscopy in order to construct ordered restriction maps of chromosomes (85). More recently, OGM has been reintroduced by BionanoGenomics[R] (San Diego, CA, US), in order to improve the cytogenetic diagnosis of germinal disorders and hematologic malignancies. The novel system is based on the extraction of ultra-high molecular weight (UHMW) DNA (i.e. 20 Kb) from any biologic sample, e.g. bone marrow, peripheral blood or solid tissue. The big amount of genomic material is required to ensure a coverage of at least 300x. Increased number of sequencing reads results in increased sensitivity, compared with RT, leading to detection of low rate alterations (86). UHMW DNA extraction relies on the properties of isopropanolol for precipitation and on the negative electrical charge of the separated DNA for capture by beads. If an adequate amount of DNA is available, the fluorescent labelling is performed. This step is possible due to Direct Label Enzyme (DLE-1) binding to a specific sequence (CTTAAG), occurring approximately every five Kb. The labelled DNA is loaded on a chip characterized by nano-channels with decreasing diameter to unfold and linearize each molecule. The long molecules are then imaged by Saphyr instrument which is equipped with a complex system of lens to magnify and capture the UHMW-DNA flowing through nano-channels. The result is images with unique labelling pattern which can be processed bioinformatically and assembled into the optical consensus map of the patient (Figure 7). Genome construction is achieved via different pipelines depending on the pathology under investigation. To date, *de novo* assembly and rare variant assembly are available. The former arranges all the labelled molecules into a whole genome which is compared with a reference map; the latter creates clusters of molecules based on the similar labelling pattern and compared with reference aggregates. Therefore, *de novo* assembly is able to detect very small SVs but could miss rare events; rare variant pipeline could underestimate low size aberrations but is able to identify both CNVs and SVs with a VAF threshold of about 10% and 5%, respectively. Consequently, the first pipeline is mostly indicated for constitutional assessment while the second one is the gold standard for evaluation of hematologic malignancies, due to high rate of mosaicism (i.e. aberration with very low VAF) in the tumor sample.

Figure 7- Schematic representation of optical genome mapping workflow. Ultra-high molecular weight DNA is extracted, labelled with DLE-1 enzyme and loaded on a chip, then imagined by Sapphyre instrument (BionanoGenomics). Images are assembled into the optical consensus map of the patient by disease-specific pipelins and compared with the corresponding images from healthy controls.
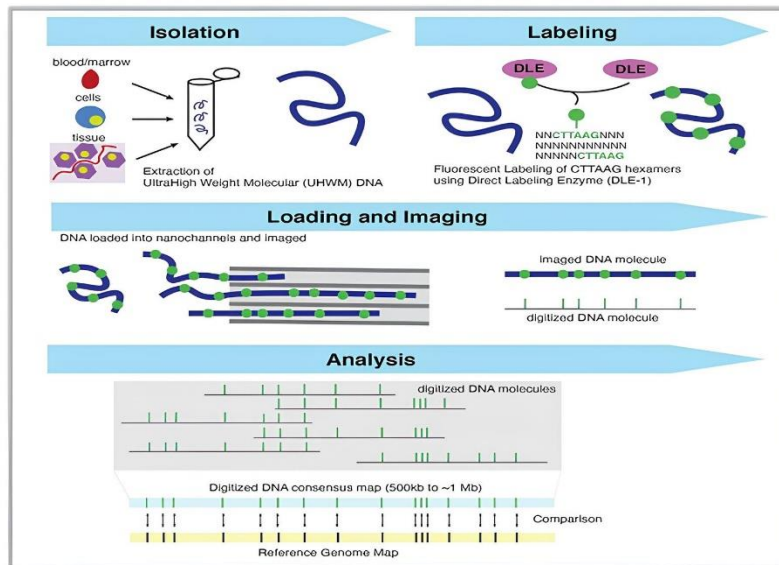


Figure modified from Kim KS, et al. Arch Pathol Lab Med. 2023 Aug.

8.2.b Application in haematological diagnostics

Due to its ability to identify both CNVs and SVs, OGM could be applied to the study of all hematologic malignancies characterized by a great genetic variability.

- AML: OGM proved to be very effective in the refinement of cytogenetic diagnosis of AML, since it enables detection of cryptic translocations leading to gene fusions with prognostic impact, such as *MECOM::ETV6* and *NSD1::NUP98* (87). Furthermore, it could improve identification of chromosome breakpoints involved in translocations, providing a more accurate description of karyotyping (88).

- MDS: OGM could also be very useful in supplementing RT in the diagnosis of MDS. An American study performed on a consecutive series of 101 cases of newly diagnosed MDS showed its ability to detect novel alterations in 34% of patients, with dramatic changes on risk-stratification according both to R-IPSS and Comprehensive Cytogenetic Scoring System (CCSS) (89).

- multiple myeloma (MM): plasma-cell neoplasms are characterized by the progressive accretion of genetic lesions, with progressive occurrence of catastrophic events, namely chromotripsis, which is difficult to assess by RT. Actually, two independent studies have recently shown that OGM is useful for the detection of both driver and secondary aberrations (e.g. *IGH* rearrangements and *TP53* deletion, respectively). Furthermore, it could provide larger pangenomic information which could impact prognosis (90, 91).

- chronic lymphocytic leukemia (CLL): risk stratification in CLL generally relies on FISH panels that should be supplemented with other standard tests for a more comprehensive genome view. OGM could be a valid alternative since it could identify both known and novel aberrations, contributing to the definition of cases with complex karyotype and worse prognosis (92).

- myeloproliferative neoplasms (MPNs): in the wide range of MPNs, OGM finds application mainly in diseases characterized by cryptic alterations and complex genetic landscapes, such as hyper eosinophilic syndromes. Indeed, a study has already showed that this novel tool could be helpful for the identification of rare partner genes involved in *PDGFRB* fusions (93) and many other trials are ongoing to dissect the aberrations of these hard-to-diagnose diseases.

- ALL: as previously discussed, the aberrations underlying onset and evolution of ALL are numerous and only a few resulting in impaired outcomes have been identified, especially in the adult population. To date, many studies have been published by different cooperative groups, evaluating the application of OGM in the cytogenetic diagnosis of both pediatric and adult T- and B-ALL (94, 95, 96). In all of them, OGM enables the detection of further aberrations and provides a more accurate description of karyotype compared to RT, including in some cases genomic

micro-array and massive sequencing strategies, such as whole genome and exome sequencing. However, it misses the detection of alterations affecting chromosomal regions with repeated sequences, such as *CRLF2* in Xp22.3, impairing the diagnosis of Ph-like cases.

## 8.3 Digital multiplex ligation dependent-probe amplification

### 8.3.a General principles

dMLPA is developed by MRC Holland[R] (Amsterdam, NL) from standard MLPA (sMLPA), considered as one of the methods of choice for detection of CNVs, since its introduction in 2002 (97). With regard to the sMLPA, a minimum target DNA of 40 μg is mixed with a maximum of 60 disease-specific fluorescent-labelled probes. Each of them consists of two pieces binding to immediately adjacent targets of sample DNA. Therefore, after overnight hybridization, treatment with ligase will ensure subsequent amplification by PCR only of probes that have hybridized perfectly; actually, in case of base mismatches, enzymatic ligation will be abortive and PCR will generate copies of small fragments which could be missed by reading methods. The standard detection method is represented by capillary electrophoresis: each amplicon passing through a capillary channel emits a fluorescent peak; the area of each of these peaks is compared with the corresponding area in the standard population to determine any losses or gains. In the digital variant, the quantification is via Illumina (San Diego, CA, US) NGS technology. The absolute read numbers of the probe amplicons provided by this tool is compared by bioinformatics software with reference samples to obtain probe ratios: since a normal ratio of 1.0 indicates normal copy number (2n), all values above or below will indicate a gain or a loss, respectively (Figure 8). Use of NGS-based quantification allows use of lower amount of DNA (i.e. 20 μg) and hybridization with of up to 1000 probes in a single reaction, in contrast to the standard method. In particular, the reaction mix include both specific probes to regions usually affected by CNVs in B-ALL and karyotyping probes to highly preserved regions for detection of massive ploidy changes and for reference during data normalization. Furthermore, recurrent point mutations (e.g. *TP53*, *IKZF1*, *NOTCH1*) can be identified if probes complementary to the mutated sequences are used: in this case, the absence of amplicons will indicate the presence of a wild-type sequence.

Figure 8. Schematic representation of digital multiplex ligation dependent-probe amplification. Target DNA is hybridized with probes, each consisting of two pieces binding to immediately adjacent targets of sample DNA (A). After overnight hybridisation, ligation ensures that only perfectly hybridised probes are amplified by PCR (B, C). The amplicons are quantified by next-generation sequencing and the read counts are bioinformatically compared to the reference samples in order to obtain the probe ratios: all the values above or below the normal range indicate a gain or a loss, respectively (D, E).
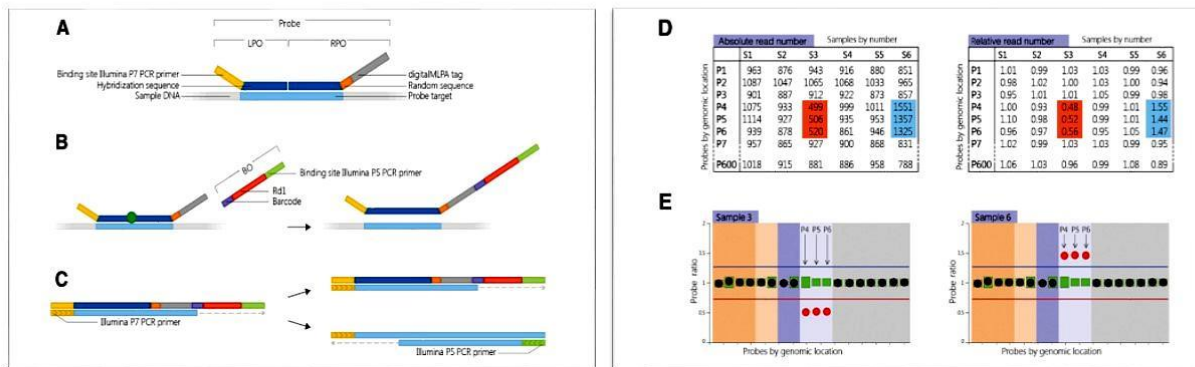


Figure modified from Benard-Slagter A, et al. JMD. 2017 Sep.

8.3.b Applications in hematological diagnostics

The application of dMLPA is limited by its ability to detect only CNVs and SVs due to interstitial deletion. Therefore, this novel tool has being implemented mostly in the context of hematologic malignancies affected by several CNVs, such as B-ALL. Indeed, this technique was firstly developed on 67 samples from B or T-ALL patients, previously characterized by RT (98). In all cases, it detected whole chromosomes or genes deletions and gains, included sub clonal alterations if present in at least 20% to 30% of blasts. This data was later confirmed by a study performed on BM samples at baseline from 91 pediatric patients (99). For 24 of them, samples at relapse were also available and different patterns of clonal evolution of CNVS were identified by their comparison with the matched diagnostic specimens. More recently, the application of dMLPA to a large cohort of adult patients led to detection of recurrent gains and losses not only in the well-known genes driving leukemogenesis but also in other regions, such as *RUNX1*, *LEF1*, *NR3C2*, *PAR1*, *PHF6*, *NF1*, *SUZ12*, *MTAP* (100). These CNVs seem to correlate with the status of MRD clearance and could help identification of novel ALL subsets.

9. Aim of the study

Briefly, based on data from literature, both OGM and dMLPA could successfully integrate RT for the cytogenetic characterization of adult B-ALL. The implementation of these tools is required since many aberrations are still unknown, but their identification could refine the risk-stratification at baseline and unveil drug-attackable targets, with dramatic improvement of prognosis. To the best of our knowledge, no comparison or integration has yet been made between OGM and dMLPA. Therefore, we aimed to evaluate their feasibility and diagnostic value in a real-life setting of ALL previously characterized by RT.

## 10. Materials and methods

For the purpose of the study, we selected a cohort of newly diagnosed adult B-ALL patients with sufficient leftover material after cytogenetic routine testing (RT) (i.e. CBA, FISH and genomic microarray).

OGM was performed in Spain following manufacturer's instructions (BionanoGenomics[R], San Diego, CA, US). The protocol consisted of two days. The first day was dedicated to UHMW-DNA extraction. This could come from bone marrow or peripheral blood, either frozen or fresh, or from frozen pellets, depending on the availability of biological material. The minimum amount of cells required to proceed with the extraction was 1.5 million, regardless of the starting sample. The cell count was performed by HemoCue[R] technology (Angelholm, SE). For DNA isolation, the specimen was treated with proteinase K; the lysate was then transferred to a specific tube, combined with NanoBind Disk and rotated on HulaMixer[TM] in order to allow the DNA within the lysate to adhere to the disk surface. Any non-genomic residue was washed away by applying a buffer to the tube mounted on a magnetic rack, thus isolating the DNA bound to the disk. Subsequently, the disk with the purified genetic material was transferred by Bionano Prep SP Magnetic Retriever into another specific tube and further washed to elute the DNA. The genetic material was then homogenized by slowly pipetting and incubated overnight at room temperature. The following day, the UHMW-DNA was quantified by Qubit[R] technology (Waltham, MA, US). If 150 ng/μl were collected, we proceeded with staining 750 ng using DLE-1 and DL-green. After, the stained UHMW-DNA was loaded onto the activated chip and run on Sapphyre instrument for maximum three days. The success of the run was evaluated by considering the following quality parameters:

- Total amount of DNA from molecules that are 20 kb or longer ≥ 20 Kb= 516.18 Gb;
- N50 (weighted average length of DNA molecules in the dataset) ≥ 150 Kb;
- Map rate (percentage of molecules aligning to the reference) > 70%;
- Average label density (average number of labels per 100 kbp for the molecules that are 150kbp or longer) 14-17/100 Kb;
- Positive label variance (percentage of labels absent in reference) < 10
- Negative label variance (percentage of reference labels absent in molecules) < 15.

Data analysis was carried out through rare variant analysis algorithm on BionanoSolve software (v3.7), using GRCh37/h19 as genome reference. SVs and CNVs were visualized on Bionano Access (v.1.7.1) by circus plot, genome browser and ideogram tools and only considered if overlapping with regions included in open-access BED files for B-ALL or if ≥ 100 kb.

dMLPA experiments were performed in Italy according to manufacturer's instructions (MRC Holland, Amsterdam, NL). For each reaction, an amount of DNA between 20 and 250 ng, extracted by commercial kit,

was required. The protocol consisted of two days. On the first day, each DNA sample was barcoded and denatured through thermocycler, then hybridized with specific digitalMLPA probe mix. In particular, for the aim of the study, we used D007 Acute Lymphoblastic Leukemia probemix, including 347 target probes detecting CNV involved in ALL and 249 karyotyping probes. After overnight hybridization, the sample-specific products underwent ligation reaction and amplification by PCR. Amplification of quality control probes present in the probe mix were evaluated to ensure the reliability of the results. For amplicon quantification, equal amounts of each PCR reaction were combined in a single tube and loaded on an Illumina MiSeq V3 flow-cell. Data analysis was performed through bioinformatics software provided by manufacturer. For each sample, the results were displayed as a chart, with x-axis representing the probes along the genome and y-axis representing the read ratio as compared with the reference samples. The interpretation was based on the principle that, in a sample with 100% tumor infiltration consisting of only one clone, a read ratio of 1.0 indicated normal copy number for autosomal and pseudo autosomal gene regions, a read ratio of 0.5 indicated a heterozygous deletion, and a read ratio of 1.5 indicated a gain of one copy. For the remaining parts of X and Y-chromosomes, the normal copy number was considered one, based on the male sex of the reference.

## 11. Results

Twenty cases were collected from May 2023 to July 2024. Median age was 50 years (range 18-70). The male/female ratio was 1:1. Based on RT, 10 patients (50%) were classified as NOS, by both ICC and WHO classifications and six cases (30%) had a Ph-like profile. Within this last category, applying the most recent revision of ICC, 4 patients exhibited an expression profile compatible with activation of the JAK-STAT pathway [t(X;14)(p22;q32)/*IGH::CRLF2*: 1 case; del(X)(p22;p22)/*CRLF2::P2RY8*: 2 cases; inv(9)(p24)/*JAK2::?*: 1 case] , 1 had an *ABL1*-class rearrangement, and 1 had an *FGFR1* rearrangement, belonging to the Ph-like, NOS subtype. Of the remaining four patients, 1 had *KMT2A*-r [t(4;11)(q21;q23)], 1 had *PBX1*-r [t(1;19)(q23;p13)], 1 had a complex karyotype corresponding to endo-reduplicated hypodiploidy, and 1 had a PAX5 P80R mutation, recognized as a distinct entity by ICC but classified within the group "with other defined genetic abnormalities" according to WHO (Table 4).

Table 4- Cytogenetic findings based on routine testing.

| No. of case | Age | Sex | G-banding analysis | FISH analysis | SNP-array analysis | WHO 2022 category | ICC 2022 category |
|---|---|---|---|---|---|---|---|
| 1 | 29 | M | 46,XY | *CRLF2*-r | *IKZF1* 2n<br>*CDKN2A/B* n | *BCR::ABL*-like features | *BCR:ABL*-like, JAK-STAT activated |
| 2 | 18 | M | 46,XY | *CRLF2* wt | *IKZF1* 2n<br>*CDKN2A/B* 2n | NOS | Without recurrent abnormalities |
| 3 | 31 | F | 46,XX,del(12)(p12),del(16)(q22), del(6)(q21q25),add(9)(p22), del(11)(q21), del(12)(p12),del(16)(q22), i(17)(q10) | *CRLF2* wt<br>*TP53*-del (borderline) | *IKZF1* 2n<br>*CDKN2A/B* n | NOS | Without recurrent abnormalities |
| 4 | 21 | F | 46,XX,-20,+mar | *CRLF2* wt | *IKZF1* 2n<br>*CDKN2A/B* n | NOS | Without recurrent abnormalities |
| 5 | 70 | F | 47,XX,+13 | *CRLF2*-r | na | *BCR::ABL*-like features | *BCR:ABL*-like, JAK-STAT activated |
| 6 | 55 | M | 46,XY,t(4;11)(q21;q23) | *KMT2A*-r | *IKZF1* 2n<br>*CDKN2A/B* n | *KMT2A* rearranged | t(v;11q23.3)/ *KMT2A* rearranged |
| 7 | 60 | F | 46,XX,inv9(p24.1q33.3) | *JAK2*-r | na | *BCR::ABL*-like features | *BCR:ABL*-like, JAK-STAT activated |
| 8 | 45 | M | Not informative | *CRLF2* wt | na | NOS | Without recurrent abnormalities |
| 9 | 23 | M | 46,XY,del(9)(q21) | *CRLF2*-wt | *IKZF1* n<br>*CDKN2A/B* n | NOS | Without recurrent abnormalities |
| 10 | 53 | F | 46,XX,-7, t(8;22)(p11.2;q11.2),+der(8)t(8;22) | *FGFR1*-r | *IKZF1* n<br>*CDKN2A/B* 2n | *BCR::ABL*-like features | *BCR:ABL*-like, NOS |
| 11 | 60 | F | 46,XX | *CRLF2*-r | *IKZF1* n<br>*CDKN2A/B* 2n | *BCR::ABL*-like features | *BCR:ABL*-like, JAK-STAT activated |
| 12 | 42 | F | Not informative | *CRLF2* wt<br>*IGH*-r | *IKZF1* n<br>*CDKN2A/B* n | NOS | Without recurrent abnormalities |
| 13 | 22 | F | 47,XX,+12 | *CRLF2* wt | *IKZF1* n<br>*CDKN2A/B* 2n | NOS | Without recurrent abnormalities |

| 14 | 51 | F | 46,XX,del(12)(p12), del(13)(q14q22),del(16)(q24) | CRLF2-wt | IKZF1 n CDKN2A/B 2n | NOS | Without recurrent abnormalities |
|---|---|---|---|---|---|---|---|
| 15 | 50 | F | 46,XX,del(9)(p13),t(9;13)(p21;q14), der(19)t(1;19)(q23;p13.3) | TCF3-r | IKZF1 2n CDKN2A/B n | TCF3::PBX1 fusion | t(1;19) (q23.3;p13.3) / TCF3::PBX1 |
| 16 | 56 | M | Not informative | TP53-del | Endoreduplicated hypodiploidy | Hypodiploidy | Low hypodiploidy |
| 17 | 41 | F | Not informative | na | IKZF1 n CDKN2A/B n | NOS | Without recurrent abnormalities |
| 18 | 60 | F | 46,XX,t(9;?)(p13.2;?) | JAK2 wt PAX5-r | IKZF1 n CDKN2A/B 2n | With other defined abnormalities | PAX5 alteration (PE) |
| 19 | 57 | M | Not informative | JAK2-del | IKZF1 n CDKN2A/B n | NOS | Without recurrent abnormalities |
| 20 | 24 | M | 47,XXY | CRLF2-gain | IKZF1 n CDKN2A/B n del(9)(q34.11) | BCR::ABL-like features | BCR:ABL-like, ABL-1 class rearranged |

Abbreviations:

-r: rearranged; wt: wild type; del: deletion; na: not available; 2n: two gene copies; n: one gene copy; PE: provisional entity

Overall, 136 calls were reported by OGM analysis. Ninety-eight (72%) corresponded to alterations already detected by RT and 38 (28%) were identified for the first time. Instead, thirty-seven previously known aberrations (27%) were not detected by OGM. dMLPA analysis showed 104 calls: 68 (65%) were previously known, while 36 (35%) were newly identified. However, dMLPA missed 67 alterations (51%) which had been reported by RT.

Thereafter, we filtered only the calls related to pathogenic aberrations, namely those larger than 100 Kb or overlapping with genes implicated in B-leukemogenesis. OGM detected all the previously identified aneuploidies, both those resulting from duplication and those resulting from loss. It also confirmed CNVs affecting single genes, mostly *BLTA*, *IKZF1*, *CDKN2A*, *PAX5*, *RB1*, *BTG1*, *ETV6*, *VPREB1* deletions that are associated with adverse prognostic impact. However, OGM underestimated the frequency of these alterations, since it missed the detection of deletions affecting *IKZF1, BLTA, BTG1, ETV6* and *VPREB1* in a percentage of cases between 13 and 33%. Contrariwise, OGM did not detect any CNV in either *ERG1*, showed by RT and confirmed by dMLPA, or in *RUNX1* and *NOTCH1*, identified solely by dMLPA.

All autosomal SVs already reported by RT were confirmed by OGM, specifically t(4;11)(q21;q23)/*AFF1::KMT2A*, inv(9)(p24)/*JAK2::STRBP*, t(8;22)(p11.2;q11.2)/*FGFR1::BCR*, t(1;19)(q23;p13)/*PBX1::TCF3*, del(13)(q12.2)/*FLT3::PAN3*, del(9)(q34.11)/*ABL1::NUP214*. On the other hand, OGM inaccurately assessed the frequency of SVs affecting sexual chromosomes, since it missed the only case t(X;14)(p22;q32)/*IGH::CRLF2* and one of the two cases with del(X)(p22;p22)/*CRLF2::P2RY8*, erroneously assigning 2 Ph-like patients to the NOS group. OGM did not detect previously undiagnosed pathological CNVs or aneuploidies. However, it did identified new pathogenic SVs, namely 2 cases of *ZFN384*-r [t(12;16)(p13;p13)/*ZFN384::CREBBP* and t(12;22)(p13;q13)/*ZFN384::EP300*], two cases of t(14;11)(q32.33;q24.1)/*IGH::MIR100HG*, one case of t(1;5)(q22;q32)/*MEF2D::CSFR1* and one case of t(14;19)(q32;p13.1)/*IGH::EPOR*.

As such, 3 patients previously classified as NOS were re-assigned to the subgroup with other defined genetic aberrations by WHO. However, 2 of these patients were allocated to the subgroup with *ZFN384*-r and one to the subgroup with *MEF2D*-r, if ICC was used. Furthermore, the patient previously classified based on PAX5 mutation was re-stratified as Ph-like due to detection of *EPOR*-r. Even if *IGH*-r is not recognized as a distinct entity by either of the two classifications, the detection of *IGH::MIR100HG* allowed a better risk-stratification in two NOS cases. In two other NOS cases, OGM detected the novel SVs t(6;9;11)(q15;p21.3;q14.1) and t(4;20)(q25;p13) which refined the karyotype, although without playing a pathogenic role.

dMLPA detected all the known aneuploidies, both those due to duplication and those due to loss. Moreover, it identified all prognostically significant CNVs already known from RT, without missing any calls regarding *BLTA*, *IKZF1*, *CDKN2A*, *PAX5*, *RB1*, *BTG1*, *ETV6*, *VPREB1* and *ERG1.* Indeed, it also revealed novel deletions

affecting *IKZF1, BLTA, BTG1, RUNX1* and *NOTCH1*. In this way, dMLPA enabled the assignment of a case to the high genetic risk group based on the expression of the *IKZF1^plus* profile. Due to limitations inherent in the design of the technique, dMLPA was only able to identify SVs caused by intra-chromosomal deletions. Therefore, it correctly reported del(13)(q12.2)/*FLT3::PAN3*, del(9)(q34.11)/*ABL1::NUP214* and del(X)(p22;p22)/*CRLF2::P2RY8*, the latter of which was missed by OGM.

Regarding the detection of CNVs, OGM and dMLPA showed a sensitivity of 94% and 100%, respectively and a sensitivity for detection of SVs of 81% for OGM and 33% for dMLPA. The 2 techniques exhibited a specificity of 100% for both CNVs and SVs. Therefore, the concordance between OGM and dMLPA was 80% regarding the detection of CNVs and 35% for the detection of SVs.

Overall, the techniques allowed the re-stratification of four cases (20%) into different ICC and WHO subgroups compared to RT. Moreover, they provided useful information for risk-stratification in seven additional cases (35%). Thus, 11 pts (55%) benefited from the integration of these two novel tools into the cytogenetic diagnostic algorithm for adult B-ALL (Figure 9).

Figure 9- Interaction between optical genome mapping and dMLPA

| | 1 | 2 | 3 | 4 | 5 | 6 | 7 | 8 | 9 | 10 | 11 | 12 | 13 | 14 | 15 | 16 | 17 | 18 | 19 | 20 |
|---|---|---|---|---|---|---|---|---|---|---|---|---|---|---|---|---|---|---|---|---|
| RT classification | Ph-like t(X;14) | NOS | NOS | NOS | Ph-like del(X)(p22.3) | t(4;11) | Ph-like inv(9p) | NOS | NOS | Ph-like NOS | Ph-like del(X)(p22.3) | NOS | NOS | NOS | t(1;19) | Endoreduplic low hypo | NOS | PAX5 mut | NOS | Ph-like ABL1-r |
| OGM results | (orange) | (green) | (green) | (green) | (red) | (orange) | (orange) | (green) | (orange) | (orange) | (orange) | (orange) | (orange) | (orange) | (orange) | (orange) | (orange) | (green) | (orange) | (orange) |
| Additional information by OGM | | ZNF384 :: CREBBP | CK | t(4;20) | | | JAK2 :: STRBP | IGH :: MIR 100HG | ZNF384 :: EP300 | FGFR1 :: BCR | | IGH :: MIR 100HG | | | | | MEF2D :: CSFR1 | IGH :: EPOR | | |
| Missed information by OGM | | | | | delX p22.33 | | | | | | | | | | | | | | | |
| dMLPA results | (red) | (orange) | (green) | (green) | (orange) | (red) | (red) | (orange) | (orange) | (red) | (red) | (orange) | (orange) | (orange) | (red) | (orange) | (orange) | (orange) | (orange) | (orange) |
| Additional information by dMLPA | del VPREB1 NOTCH | | CK | | IKZF+/ del VPREB1 NOTCH | del ETV6 | | | | | | | | | | | | | | |
| Missed information by dMLPA | t(X;14) | ZNF384 :: CREBB | | t(4;20) | | t(4;11) | JAK2 :: STRBP | IGH :: MIR 100HG | ZNF384 :: EP300 | FGFR1 :: BCR | | IGH :: MIR100 HG | | | TCF3 :: PBX1 | | MEF2D :: CSFR1 | IGH :: EPOR | | |
| OGM/dMLPA updated classification | (light blue) | (dark blue) | (purple) | (purple) | (purple) | (light blue) | (purple) | (purple) | (dark blue) | (purple) | (light blue) | (purple) | (light blue) | (light blue) | (light blue) | (light blue) | (light blue) | (dark blue) | (light blue) | (light blue) |

Legend:

- (orange) The result is consistent with that of routine testing
- (green) The result provides more information compared to routine testing
- (red) The result provides less information compared to routine testing
- (light blue) The result does not imply a change in classification according to routine testing
- (dark blue) The result implies a change in classification according to routine testing
- (purple) The result does not imply a change in classification according to routine testing but provides a more accurate diagnosis and risk-stratification
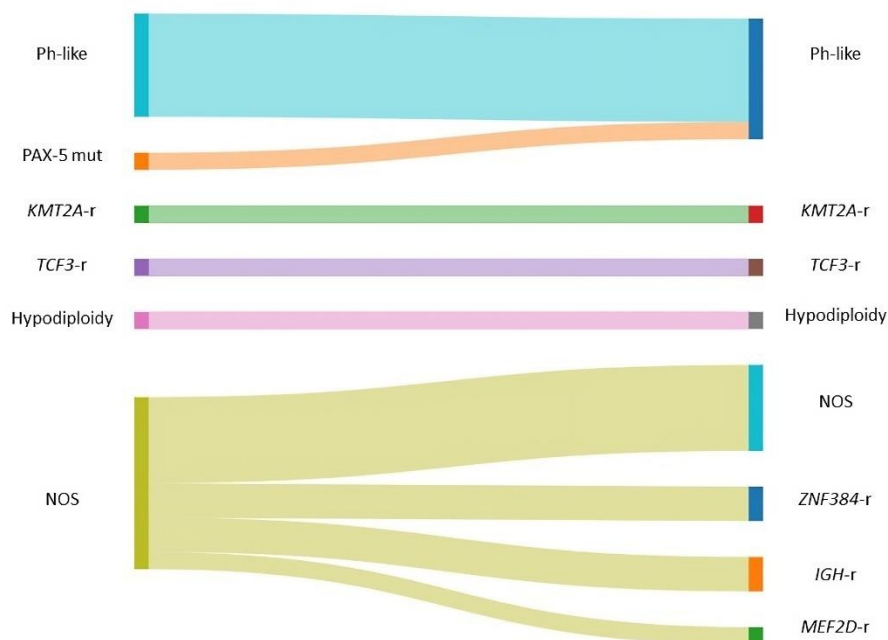
Abbreviations:

RT: routine testing; NOS: not-otherwise specified; endoreduplic low-hypo: endoreduplicated low-hypodiploidy; mut: mutated; -r: rearranged

## 12. Discussion

In our study cohort, both OGM and dMLPA proved capable to integrate the RT, providing a more accurate cytogenetic diagnosis of adult B-ALL. Indeed, in many cases, these novel tools enabled the detection of driver and non-driver pathogenic aberrations with subsequent impact on risk-stratification (Figure 10).

Figure 10. Ph-like and NOS cases benefit from application of novel cytogenetic tools for a more accurate description and risk-stratification.



Abbreviation:

-mut: mutated; -r: rearranged; NOS: not otherwise specified.

In particular, OGM outperformed standard tests for the identification of SVs. Indeed, it confirmed all the previously described balanced and unbalanced translocations affecting autosomal chromosomes but also allowed the proper identification of partners involved in rearrangements that were not fully elucidated due to the low resolution of RT.

In a Ph-like case with JAK-STAT activation based on inv(9)(p24.1q33.3), diagnosed by CBA and confirmed by FISH analysis because of a pattern consistent with JAK2 rearrangement, OGM showed that the inversion involved *STRBP*. The *STRBP-JAK2* fusion gene was previously described only in another Ph-like B-ALL patient, identified by RNA-sequencing (101). Based on the follow-up of this case, this transcript seems to induce refractoriness to conventional induction chemotherapy, even if combined with JAK2-inhibitors, and may require the use of more advanced therapies, such as CAR-T.

In another Ph-like case classified as NOS, due to the detection of t(8;22) t(8;22)(p11.2;q11.2) causing cryptic *FGFR1*-r, OGM confirmed the involvement of *BCR*. The protein-fusion arising from this juxtaposition is very rare and associated to a dismal prognosis, in spite of the potential responsiveness to TKIs (102).

In addition to confirming and redefining already known SVs, OGM also enabled the identification of novel translocations. In particular, in 2 cases classified as NOS, 1 with normal karyotype and one with del(9)(q21) without any pathologic implication, the digital technology identified *ZFN384*-r due to t(12;16)(p13;p13) and to t(12;22)(p13;q13), respectively. *ZFN384*-r are recurrent in B-other cases affecting adolescents/young adults, usually associated with co-expression of myeloid markers, $IKZF1^{plus}$profile and FLT3 mutation (18). *EP300* is the most frequent partner while *CREBBP* is more rarely involved. Even if the prognosis is still controversial, it seems to change based on the fusion partner. Actually, *ZNF384::EP300* has better outcome than *ZNF384::CREBBP* (103). Therefore, their identification by OGM allowed the reclassification of the two NOS cases into novel subgroups but also a different risk-stratification within the same category.

Another specimen classified as NOS by RT was re-stratified by the novel technology, since it detected t(1;5)(q22;q32)/*MEF2D::CSFR1*. *MEF2D*-r B-ALL is characterized by an immature phenotype and older age at onset, thus it represents a high-risk leukemia with potential sensitivity to HDAC inhibitors (104). For this reason, it has been recently incorporated into a separate entity according to ICC.

OGM also re-assigned a case previously classified based on detection of PAX5 P80R mutation by NGS. Indeed, it detected t(14;19)(q32;p13.1)/*IGH::EPOR* described as part of Ph-like signature. *EPOR*-r activate JAK-STAT pathway and could be targetable with JAK2-inhibitors even if very few data is available due to their low frequency (105).

Furthermore, in other cases considered as NOS, OGM identified pathologic SVs which refined the description of karyotype provided by CBA or the risk-stratification, although without implying a re-classification. In

particular, in a case with 20 monosomy and the presence of a large marker, the novel technology detected dup(4)(q25q35.2) and t(4;20)(q25;p13), refuting monosomy and allowing us to describe the marker as a consequence of the translocation. In another NOS case with very complex karyotype, OGM unveiled t(6;9;11)(q15;p21.3;q14.1), thus identifying the rearrangements which led to multiple gains and losses of genomic material seen by CBA. In two other cases, the tool showed the presence of t(14;11)(q32.33;q24.1)/*IGH::MIR100HG*. *MIR100HG* codes for a long non-coding RNA which seems to play a role in hematopoiesis and could act as an oncogene, favouring the onset of rare leukemias, such as the megakarioblastic form, under certain conditions (106). Therefore, in our cases, its juxtaposition to a constitutionally active gene (i.e. IGH) could imply deregulation of cell proliferation and promote disease.

OGM down performed RT for detection of SVs affecting sexual chromosomes and of CNVs affecting genes involved in B-leukemogenesis. In particular, it missed two cases of *CRLF2*-r, namely del(X)(p22;p22)/*CRLF2::P2RY8* and t(X;14)(p22;q32)/*IGH::CRLF2*, leading to underestimate the frequency of Ph-like cases. This limit seems to be due to the low coverage of chromosomal regions with repeated sequences and is concordant with other studies (94, 107-109). However, more updated versions of the analysis software could overcome this limitation and provide greater coverage of autosomal regions in sex chromosomes. OGM also missed deletions affecting *IKZF1, BLTA*, *BTG1*, *ETV6*, *VPREB*, *ERG1*, *RUNX1* and *NOTCH1*. Overall, failure to report these CNVs could impair a proper risk-stratification, due to the association of deletions in these regions with a dismal prognosis, as commented in the Introduction. In particular, the lack of detection of *IKZF1* deletion in a Ph-like patient with concomitant deletion of *CDKN2/B* did not allow the identification of $IKZF1^{plus}$ profile, that deserves a more aggressive therapeutic approach due to its negative effect on prognosis (26). The underestimation of CNVs by OGM could be due to the mechanism of analysis, since they are inferred, unlike the direct visualization of SVs.

dlMLPA is a better technique for the identification of CNVs. It is specifically designed to detect any variation in the allelic load of genes involved in the onset and progression of B-ALL. In particular, it confirmed every gain and loss previously described by RT but also detected novel aberrations affecting *RUNX1* and *NOTCH1* in two Ph-like cases. Both genes play a role in hematopoiesis and the pro-leukemic effect due to their mutation has been extensively described. However, little is known about the consequence of their deletion. *RUNX1* deletion was only associated with poor survival in pediatric AML (110). A study performed at MD Anderson showed that the aberrant expression of *NOTCH1,* also due to its deletion, is recurrent in Ph-like cases and proved in vitro that inhibition of cascade downstream NOTCH could have anti-leukemia effect (111). Therefore, we could speculate about a potential adverse prognostic role played by these novel deletions detected through dMLPA in our case-cohort. Even if OGM proved to be very effective for detection of SVs, dMLPA might be more suitable for the study of aberrations due to intra-chromosomal deletions, especially those affecting sex chromosomes. Indeed, the better coverage of *CRLF2* region provided by dMLPA

easily allowed the identification of the two cases characterized by del(X)(p22;p22)/*CRLF2::P2RY8*, without any need for a manual revision.

The implementation of the 2 techniques also entails considering the technical aspects. DNA extraction for OGM is challenging due to the required large amount of perfectly homogenised product. On the contrary, a lower quantity of DNA obtainable through commercial kits is sufficient for dMLPA. None of the two techniques relies on cell culture. They can be directly performed on both fresh and frozen samples. However, unlike OGM, dMLPA requires PCR amplification that could alter the representation of the clonal architecture in the sample on study. OGM can only be performed with specific instrumentation while, for dMLPA, the quantification can be done by NGS apparatus, simultaneously with runs of other types. Data interpretation is simple and intuitive, both with OGM software and dMLPA software, and no bioinformatics expertise is required. Therefore, even if the overall costs are medium-to-high for both techniques, long-term savings should be considered.

13. Conclusion

To the best of our knowledge, this is the first study to integrate simultaneously OGM and dMLPA in the standard cytogenetic diagnosis of adult B-ALL. Both techniques proved useful in providing a better characterization of most of the cases presented. Indeed, OGM and dMLPA outperformed RT for the detection of SVs and CNVs, respectively, showing high sensitivity and specificity, in accordance with the literature data. In particular, the two techniques ensured a more accurate description of NOS and Ph-like cases. Most of adult patients diagnosed with B-ALL belong to these categories but their intricate genetic landscape is still far to be fully elucidated and RT is not enough. Therefore, OGM and dMLPA could be applied specifically to redefine the diagnosis of these challenging cases. However, due to their recent introduction, a greater experience with larger cohorts is required to understand how they could be integrated in the cytogenetic laboratory workflow (Figure 11).

Figure 11. Algorithm showing how OGM and digitalMLPA could be integrated in the cytogenetic laboratory workflow for detection of genetic abnormalities included in EWALL score (Reference 33).
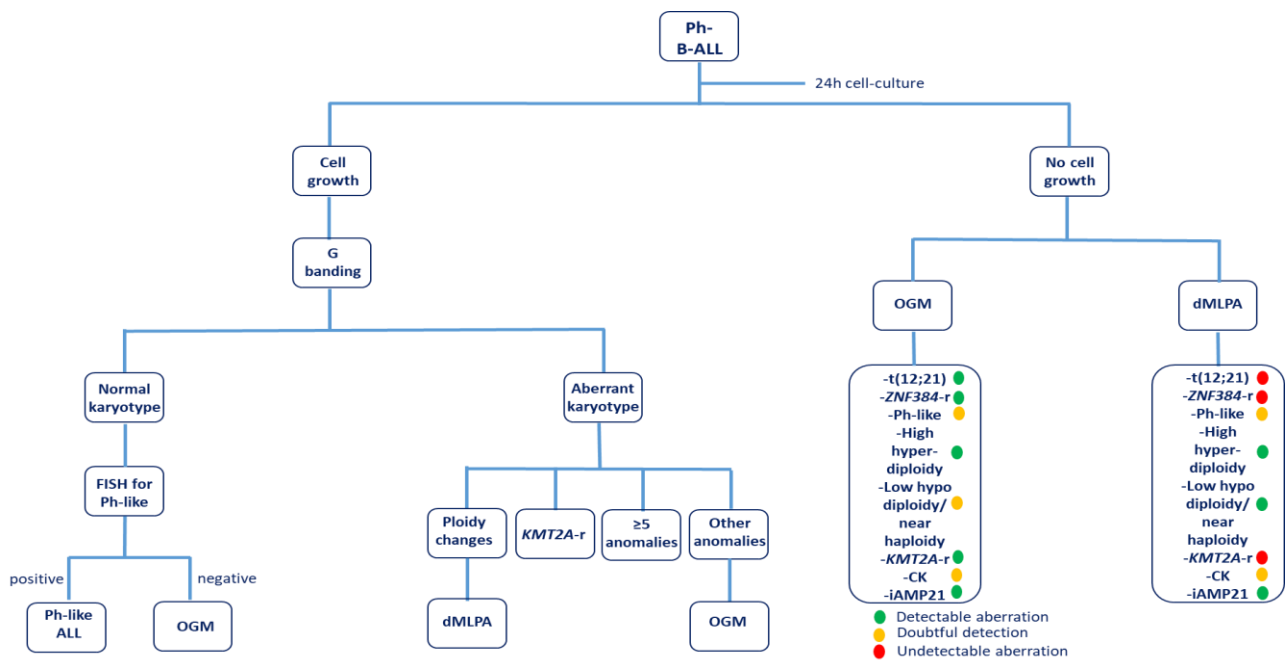
References:

1) Brown PA, Shah B, Advani A, et al. Acute Lymphoblastic Leukemia, Version 2.2021, NCCN Clinical Practice Guidelines in Oncology. J Natl Compr Canc Netw. 2021 Sep 20;19(9):1079-1109. doi: 10.6004/jnccn.2021.0042. PMID: 34551384

2) Gökbuget N, Boissel N, Chiaretti S, et al. Diagnosis, prognostic factors, and assessment of ALL in adults: 2024 ELN recommendations from a European expert panel. Blood. 2024 May 9;143(19):1891-1902. doi: 10.1182/blood.2023020794. PMID: 38295337

3) Bennett JM, Catovsky D, Daniel MT, et al. Proposals for the classification of the acute leukaemias. French-American-British (FAB) co-operative group. Br J Haematol. 1976 Aug;33(4):451-8. doi: 10.1111/j.1365-2141.1976.tb03563.x. PMID: 188440.

4) Béné MC, Nebe T, Bettelheim P, et al. Immunophenotyping of acute leukemia and lymphoproliferative disorders: a consensus proposal of the European LeukemiaNet Work Package 10. Leukemia. 2011 Apr;25(4):567-74. doi: 10.1038/leu.2010.312. Epub 2011 Jan 21. PMID: 21252983.

5) Li J, Dai Y, Wu L, et al. Emerging molecular subtypes and therapeutic targets in B-cell precursor acute lymphoblastic leukemia. Front Med. 2021 Jun;15(3):347-371. doi: 10.1007/s11684-020-0821-6. Epub 2021 Jan 5. PMID: 33400146

6) Foà R, Chiaretti S. Philadelphia Chromosome-Positive Acute Lymphoblastic Leukemia. N Engl J Med. 2022 Jun 23;386(25):2399-2411. doi: 10.1056/NEJMra2113347. PMID: 35731654

7) Meyer C, Larghero P, Almeida, et al. The KMT2A recombinome of acute leukemias in 2023. Leukemia. 2023 May;37(5):988-1005. doi: 10.1038/s41375-023-01877-1. Epub 2023 Apr 5. PMID: 37019990; PMCID: PMC10169636

8) Kaczmarska A, Derebas J, Pinkosz M, et al. The Landscape of Secondary Genetic Rearrangements in Pediatric Patients with B-Cell Acute Lymphoblastic Leukemia with t(12;21). Cells. 2023 Jan 18;12(3):357. doi: 10.3390/cells12030357. PMID: 36766699; PMCID: PMC9913634

9) Yilmaz M, Kantarjian HM, Toruner G, et al. Translocation t(1;19)(q23;p13) in adult acute lymphoblastic leukemia - a distinct subtype with favorable prognosis. Leuk Lymphoma. 2021 Jan;62(1):224-228. doi: 10.1080/10428194.2020.1824071. Epub 2020 Sep 21. PMID: 32955970

10) Tasian SK. TCF3::HLF acute lymphoblastic leukemia: still challenging to cure thirty years later. Haematologica. 2023 Jul 1;108(7):1713-1714. doi: 10.3324/haematol.2023.283148. PMID: 37392046; PMCID: PMC10316242

11) Rabin KR. Insights into the genomics of iAMP21-ALL. Blood. 2023 Aug 24;142(8):682-684. doi: 10.1182/blood.2023021020. PMID: 37616022

12) Enshaei A, Martinez Elicegui J, Anguiano E, et al. Real-world evaluation of UK high hyperdiploidy profile using a large cohort of patients provided by HARMONY data platform. Leukemia. 2023 Dec;37(12):2493-2496. doi: 10.1038/s41375-023-02046-0. Epub 2023 Sep 29. PMID: 37773265; PMCID: PMC10681889

13) Kim R, Bergugnat H, Larcher L, et al. Adult Low-Hypodiploid Acute Lymphoblastic Leukemia Emerges from Preleukemic TP53-Mutant Clonal Hematopoiesis. Blood Cancer Discov. 2023 Mar 1;4(2):134-149. doi: 10.1158/2643-3230.BCD-22-0154. PMID: 36630200; PMCID: PMC9975768

14) Duffield AS, Mullighan CG, Borowitz MJ. International Consensus Classification of acute lymphoblastic leukemia/lymphoma. Virchows Arch. 2023 Jan;482(1):11-26. doi: 10.1007/s00428-022-03448-8. Epub 2022 Nov 24. PMID: 36422706; PMCID: PMC10646822

15) Aldoss I, Gu Z, et al. Ph-like acute lymphoblastic leukemia in adults: understanding pathogenesis, improving outcomes, and future directions for therapy. Leuk Lymphoma. 2023 Jun;64(6):1092-1101. Doi:10.1080/10428194.2023.2197538. Epub 2023 Apr 6. PMID: 37021793

16) Fournier B, Balducci E, Duployez N, et al. B-ALL With t(5;14)(q31;q32); IGH-IL3 Rearrangement and Eosinophilia: A Comprehensive Analysis of a Peculiar IGH-Rearranged B-ALL. Front Oncol. 2019 Dec 10;9:1374. doi: 10.3389/fonc.2019.01374. PMID: 31921638; PMCID: PMC6914849

17) Kimura S, Montefiori L, Iacobucci I, et al. Enhancer retargeting of CDX2 and UBTF::ATXN7L3 define a subtype of high-risk B-progenitor acute lymphoblastic leukemia. Blood. 2022 Jun 16;139(24):3519-3531. doi: 10.1182/blood.2022015444. PMID: 35192684; PMCID: PMC9203703

18) Chiaretti S, Taherinasab A, Della Starza I, et al. ZNF384 rearrangement is the most frequent genetic lesion in adult PH-negative and Ph-like-negative B-other acute lymphoblastic leukemia. Biological and clinical findings. Leuk Lymphoma. 2023 Feb;64(2):483-486. doi: 10.1080/10428194.2022.2148217. Epub 2022 Dec 19. PMID: 36533589

19) Gu Z, Churchman ML, Roberts KG, et al. PAX5-driven subtypes of B-progenitor acute lymphoblastic leukemia. Nat Genet. 2019 Feb;51(2):296-307. doi: 10.1038/s41588-018-0315-5. Epub 2019 Jan 14. PMID: 30643249; PMCID: PMC6525306

20) Vairy S, Tran TH. IKZF1 alterations in acute lymphoblastic leukemia: The good, the bad and the ugly. Blood Rev. 2020 Nov;44:100677. doi: 10.1016/j.blre.2020.100677. Epub 2020 Mar 31. PMID: 32245541

21) Murthy A, Lee B, Zavala A, Tirado CA. ETV6::RUNX1-like Acute Lymphoblastic Leukemia. J Assoc Genet Technol. 2024;50(2):61-63. PMID: 38824653

22) Li JF, Dai YT, Lilljebjörn H, et al. Transcriptional landscape of B cell precursor acute lymphoblastic leukemia based on an international study of 1,223 cases. Proc Natl Acad Sci U S A. 2018 Dec 11;115(50):E11711-E11720. doi: 10.1073/pnas.1814397115. Epub 2018 Nov 28. PMID: 30487223; PMCID: PMC6294900

23) Zaliova M, Winkowska L, Stuchly J, et al. A novel class of ZNF384 aberrations in acute leukemia. Blood Adv. 2021 Nov 9;5(21):4393-4397. doi: 10.1182/bloodadvances.2021005318. PMID: 34529760; PMCID: PMC8579251

24) Alaggio R, Amador C, Anagnostopoulos I, et al; International Agency for Research on Cancer/World Health Organization. Correction: "The 5th edition of The World Health Organization Classification of Haematolymphoid Tumours: Lymphoid Neoplasms" Leukemia. 2022 Jul;36(7):1720-1748. Leukemia. 2023 Sep;37(9):1944-1951. doi: 10.1038/s41375-023-01962-5. Erratum for: Leukemia. 2022 Jul;36(7):1720-1748. doi: 10.1038/s41375-022-01620-2. PMID: 37468552; PMCID: PMC10457187.

25) Moorman AV, Enshaei A, Schwab C, et al. A novel integrated cytogenetic and genomic classification refines risk stratification in pediatric acute lymphoblastic leukemia. Blood. 2014 Aug 28;124(9):1434-44. doi: 10.1182/blood-2014-03-562918. Epub 2014 Jun 23. PMID: 24957142

26) Stanulla M, Dagdan E, Zaliova M, et al. IKZF1[plus] Defines a New Minimal Residual Disease-Dependent Very-Poor Prognostic Profile in Pediatric B-Cell Precursor Acute Lymphoblastic Leukemia. J Clin Oncol. 2018 Apr 20;36(12):1240-1249. doi: 10.1200/JCO.2017.74.3617. Epub 2018 Mar 2. PMID: 29498923

27) Ribera J, Morgades M, Zamora L, et al. Prognostic significance of copy number alterations in adolescent and adult patients with precursor B acute lymphoblastic leukemia enrolled in PETHEMA protocols. Cancer. 2015 Nov 1;121(21):3809-17. doi: 10.1002/cncr.29579. Epub 2015 Jul 20. PMID: 26194343

28) Ribera J, Zamora L, Morgades M, et al. Molecular profiling refines minimal residual disease-based prognostic assessment in adults with Philadelphia chromosome-negative B-cell precursor acute lymphoblastic leukemia. Genes Chromosomes Cancer. 2019 Nov;58(11):815-819. doi: 10.1002/gcc.22788. Epub 2019 Aug 7. PMID: 31340073

29) Messina M, Chiaretti S, Fedullo AL, et al. Clinical significance of recurrent copy number aberrations in B-lineage acute lymphoblastic leukaemia without recurrent fusion genes across age cohorts. Br J Haematol. 2017 Aug;178(4):583-587. doi: 10.1111/bjh.14721. Epub 2017 Apr 25. PMID: 28439887

30) Chiaretti S, Messina M, Della Starza I, et al. Philadelphia-like acute lymphoblastic leukemia is associated with minimal residual disease persistence and poor outcome. First report of the minimal residual disease-oriented GIMEMA LAL1913. Haematologica. 2021 Jun 1;106(6):1559-1568. doi: 10.3324/haematol.2020.247973. PMID: 32467145; PMCID: PMC8168510.

31) Foà R, Bassan R, Vitale A, et al. Dasatinib-Blinatumomab for Ph-Positive Acute Lymphoblastic Leukemia in Adults. N Engl J Med. 2020 Oct 22;383(17):1613-1623. doi: 10.1056/NEJMoa2016272. PMID: 33085860.

32) Foà R, Bassan R, Elia L, et al. Long-Term Results of the Dasatinib-Blinatumomab Protocol for Adult Philadelphia-Positive ALL. J Clin Oncol. 2024 Mar 10;42(8):881-885. doi: 10.1200/JCO.23.01075. Epub 2023 Dec 21. PMID: 38127722; PMCID: PMC10927329.

33) Enshaei A, Joy M, Butler E, et al. A robust and validated integrated prognostic index for defining risk groups in adult acute lymphoblastic leukemia: an EWALL collaborative study. Blood Adv. 2024 Mar 12;8(5):1155-1166. doi: 10.1182/bloodadvances.2023011661. PMID: 38113467; PMCID: PMC10910126

34) Knudson AG Jr. Mutation and cancer: statistical study of retinoblastoma. Proc Natl Acad Sci U S A. 1971 Apr;68(4):820-3. doi: 10.1073/pnas.68.4.820. PMID: 5279523; PMCID: PMC389051

35) Malard F, Mohty M. Acute lymphoblastic leukaemia. Lancet. 2020 Apr 4;395(10230):1146-1162. doi: 10.1016/S0140-6736(19)33018-1. PMID: 32247396

36) Moriyama T, Relling MV, Yang JJ. Inherited genetic variation in childhood acute lymphoblastic leukemia. Blood. 2015 Jun 25;125(26):3988-95. doi: 10.1182/blood-2014-12-580001. Epub 2015 May 21. PMID: 25999454; PMCID: PMC4481591

37) Onyije FM, Olsson A, Baaken D, et al. Environmental Risk Factors for Childhood Acute Lymphoblastic Leukemia: An Umbrella Review. Cancers (Basel). 2022 Jan 13;14(2):382. doi: 10.3390/cancers14020382. PMID: 35053543; PMCID: PMC877359

38) Duesberg P, Li R, Fabarius A, Hehlmann R. The chromosomal basis of cancer. Cell Oncol. 2005;27(5-6):293-318. doi: 10.1155/2005/951598. PMID: 16373963; PMCID: PMC4615177

39) Tanaka K, Hirota T. Chromosome segregation machinery and cancer. Cancer Sci. 2009 Jul;100(7):1158-65. doi: 10.1111/j.1349-7006.2009.01178.x. Epub 2009 Apr 21. PMID: 19432891

40) Hosea R, Hillary S, Naqvi S, et al. The two sides of chromosomal instability: drivers and brakes in cancer. Signal Transduct Target Ther. 2024 Mar 29;9(1):75. doi: 10.1038/s41392-024-01767-7. PMID: 38553459; PMCID: PMC10980778

41) Hunger SP, Mullighan CG. Acute Lymphoblastic Leukemia in Children. N Engl J Med. 2015 Oct 15;373(16):1541-52. doi: 10.1056/NEJMra1400972. PMID: 26465987

42) Roberts KG, Gu Z, Payne-Turner D, et al. High Frequency and Poor Outcome of Philadelphia Chromosome-Like Acute Lymphoblastic Leukemia in Adults. J Clin Oncol. 2017 Feb;35(4):394-401. doi: 10.1200/JCO.2016.69.0073. Epub 2016 Nov 21. PMID: 27870571; PMCID: PMC5455698

43) Creasey T, Barretta E, Ryan SL, et al. Genetic and genomic analysis of acute lymphoblastic leukemia in older adults reveals a distinct profile of abnormalities: analysis of 210 patients from the UKALL14 and UKALL60+ clinical trials. Haematologica. 2022 Sep 1;107(9):2051-2063. doi: 10.3324/haematol.2021.279177. PMID: 34788984; PMCID: PMC9425332

44) Webster A, Schuh M. Mechanisms of Aneuploidy in Human Eggs. Trends Cell Biol. 2017 Jan;27(1):55-68. doi: 10.1016/j.tcb.2016.09.002. Epub 2016 Oct 20. PMID: 27773484

45) Matsubara K, Yanagida K, Nagai T, Kagami M, Fukami M. De Novo Small Supernumerary Marker Chromosomes Arising From Partial Trisomy Rescue. Front Genet. 2020 Feb 27;11:132. doi: 10.3389/fgene.2020.00132. PMID: 32174976; PMCID: PMC7056893

46) Liu S, Zhang K, Song F, Yang Y, Lv Y, Gao M, Liu Y, Gai Z. Uniparental Disomy of Chromosome 15 in Two Cases by Chromosome Microarray: A Lesson Worth Thinking. Cytogenet Genome Res. 2017;152(1):1-8. doi: 10.1159/000477520. Epub 2017 Jun 24. PMID: 28647735

47) Robinson WP. Mechanisms leading to uniparental disomy and their clinical consequences. Bioessays. 2000 May;22(5):452-9. doi: 10.1002/(SICI)1521-1878(200005)22:5<452::AID-BIES7>3.0.CO;2-K. PMID: 10797485

48) Eggermann T, Monk D, de Nanclares GP, et al. Imprinting disorders. Nat Rev Dis Primers. 2023 Jun 29;9(1):33. doi: 10.1038/s41572-023-00443-4. PMID: 37386011

49) Yang Y, Muzny DM, Xia F, et al. Molecular findings among patients referred for clinical whole-exome sequencing. JAMA. 2014 Nov 12;312(18):1870-9. doi: 10.1001/jama.2014.14601. PMID: 25326635; PMCID: PMC4326249

50) Epum EA, Haber JE. DNA replication: the recombination connection. Trends Cell Biol. 2022 Jan;32(1):45-57. doi: 10.1016/j.tcb.2021.07.005. Epub 2021 Aug 9. PMID: 34384659; PMCID: PMC8688190

51) Belan O, Anand R, Boulton SJ. Mechanism of mitotic recombination: insights from C. elegans. Curr Opin Genet Dev. 2021 Dec;71:10-18. doi: 10.1016/j.gde.2021.06.005. Epub 2021 Jun 26. PMID: 34186335; PMCID: PMC8683258

52) Cavenee WK, Dryja TP, Phillips RA, et al. Expression of recessive alleles by chromosomal mechanisms in retinoblastoma. Nature. 1983 Oct 27-Nov 2;305(5937):779-84. doi: 10.1038/305779a0. PMID: 6633649

53) Luo L, Chen J, Du Q, et al. A region close to Tp53 shows CN-LOH in familial breast cancer. Int J Mol Med. 2002 Apr;9(4):405-9. PMID: 11891537

54) Vieira de Oliveira SF, Oliveira MM, Urban CA, et al. Lack of association between CN-LOH in the 9p region and clinicopathologic parameters in primary breast cancer. Cancer Genet Cytogenet. 2010 Jul 1;200(1):23-7. doi: 10.1016/j.cancergencyto.2010.03.002. PMID: 20513530

55) Jänne PA, Li C, Zhao X, Girard L, et al. High-resolution single-nucleotide polymorphism array and clustering analysis of loss of heterozygosity in human lung cancer cell lines. Oncogene. 2004 Apr 8;23(15):2716-26. doi: 10.1038/sj.onc.1207329. PMID: 15048096

56) Teh MT, Blaydon D, Chaplin T, et al. Genomewide single nucleotide polymorphism microarray mapping in basal cell carcinomas unveils uniparental disomy as a key somatic event. Cancer Res. 2005 Oct 1;65(19):8597-603. doi: 10.1158/0008-5472.CAN-05-0842. PMID: 16204023

57) Walsh CS, Ogawa S, Scoles DR, et all. Genome-wide loss of heterozygosity and uniparental disomy in BRCA1/2-associated ovarian carcinomas. Clin Cancer Res. 2008 Dec 1;14(23):7645-51. doi: 10.1158/1078-0432.CCR-08-1291. PMID: 19047089; PMCID: PMC2677417

58) Howarth K, Ranta S, Winter E, et al. A mitotic recombination map proximal to the APC locus on chromosome 5q and assessment of influences on colorectal cancer risk. BMC Med Genet. 2009 Jun 10;10:54. doi: 10.1186/1471-2350-10-54. PMID: 19515250; PMCID: PMC2705358

59) O'Keefe C, McDevitt MA, Maciejewski JP. Copy neutral loss of heterozygosity: a novel chromosomal lesion in myeloid malignancies. Blood. 2010 Apr 8;115(14):2731-9. doi: 10.1182/blood-2009-10-201848. Epub 2010 Jan 27. PMID: 20107230; PMCID: PMC2854422

60) Plo I, Nakatake M, Malivert L, et al. JAK2 stimulates homologous recombination and genetic instability: potential implication in the heterogeneity of myeloproliferative disorders. Blood. 2008 Aug 15;112(4):1402-12. doi: 10.1182/blood-2008-01-134114. Epub 2008 May 30. PMID: 18515659

61) Koh KN, Lee JO, Seo EJ, et al. Clinical significance of previously cryptic copy number alterations and loss of heterozygosity in pediatric acute myeloid leukemia and myelodysplastic syndrome determined using combined array comparative genomic hybridization plus single-nucleotide polymorphism microarray analyses. J Korean Med Sci. 2014 Jul;29(7):926-33. doi: 10.3346/jkms.2014.29.7.926. Epub 2014 Jul 11. PMID: 25045224; PMCID: PMC4101780

62) Saxe D, Seo EJ, Bergeron MB, Han JY. Recent advances in cytogenetic characterization of multiple myeloma. Int J Lab Hematol. 2019 Feb;41(1):5-14. doi: 10.1111/ijlh.12882. Epub 2018 Jul 3. PMID: 29971938

63) Bea S, Salaverria I, Armengol L, et al. Uniparental disomies, homozygous deletions, amplifications, and target genes in mantle cell lymphoma revealed by integrative high-resolution whole-genome profiling. Blood. 2009;113(13):3059-3069

64) Mullighan CG, Goorha S, Radtke I, et al. Genome-wide analysis of genetic alterations in acute lymphoblastic leukaemia. Nature. 2007 Apr 12;446(7137):758-64. doi: 10.1038/nature05690. PMID: 17344859

65) Kawamata N, Ogawa S, Zimmermann M, et al. Molecular allelokaryotyping of pediatric acute lymphoblastic leukemias by high-resolution single nucleotide polymorphism oligonucleotide genomic microarray. Blood. 2008 Jan 15;111(2):776-84. doi: 10.1182/blood-2007-05-088310. Epub 2007 Sep 21. PMID: 17890455; PMCID: PMC2200831

66) Sulong S, Moorman AV, Irving JA, et al. A comprehensive analysis of the CDKN2A gene in childhood acute lymphoblastic leukemia reveals genomic deletion, copy number neutral loss of heterozygosity, and association with specific cytogenetic subgroups. Blood. 2009 Jan 1;113(1):100-7. doi: 10.1182/blood-2008-07-166801. Epub 2008 Oct 6. PMID: 18838613

67) Hosking FJ, Papaemmanuil E, Sheridan E, et al. Genome-wide homozygosity signatures and childhood acute lymphoblastic leukemia risk. Blood. 2010 Jun 3;115(22):4472-7. doi: 10.1182/blood-2009-09-244483. Epub 2010 Mar 15. PMID: 20231427

68) Lundin KB, Olsson L, Safavi S, et al. Patterns and frequencies of acquired and constitutional uniparental isodisomies in pediatric and adult B-cell precursor acute lymphoblastic leukemia. Genes Chromosomes Cancer. 2016 May;55(5):472-9. doi: 10.1002/gcc.22349. Epub 2016 Feb 4. PMID: 26773847

69) Sinclair PB, Ryan S, Bashton M, et al. SH2B3 inactivation through CN-LOH 12q is uniquely associated with B-cell precursor ALL with iAMP21 or other chromosome 21 gain. Leukemia. 2019 Aug;33(8):1881-1894. doi: 10.1038/s41375-019-0412-1. Epub 2019 Feb 28. PMID: 30816328; PMCID: PMC6756024

70) Risinskaya N, Gladysheva M, Abdulpatakhov A, et al. DNA Copy Number Alterations and Copy Neutral Loss Genes of Heterozygosity in Adult Ph-Negative Acute B-Lymphoblastic Leukemia: Focus on the Involved. Int J Mol Sci. 2023 Dec 18;24(24):17602. doi: 10.3390/ijms242417602. PMID: 38139431; PMCID: PMC10744257

71) Song J, Shao H. SNP Array in Hematopoietic Neoplasms: A Review. Microarrays (Basel). 2015 Dec 22;5(1):1. doi: 10.3390/microarrays5010001. PMID: 27600067; PMCID: PMC5003446

72) Gochi L, Kawai Y, Fujimoto A. Comprehensive analysis of microsatellite polymorphisms in human populations. Hum Genet. 2023 Jan;142(1):45-57. doi: 10.1007/s00439-022-02484-3. Epub 2022 Sep 1. PMID: 36048238

73) Dai S, Long Y. Genotyping analysis using an RFLP assay. Methods Mol Biol. 2015;1245:91-9. doi: 10.1007/978-1-4939-1966-6_7. PMID: 25373751

74) Dougherty MJ, Wilmoth DM, Tooke LS, et al. Implementation of high resolution single nucleotide polymorphism array analysis as a clinical test for patients with hematologic malignancies. Cancer Genet. 2011 Jan;204(1):26-38. doi: 10.1016/j.cancergencyto.2010.10.007. PMID: 21356189

75) Schoumans J, Suela J, Hastings R, et al. Guidelines for genomic array analysis in acquired haematological neoplastic disorders. Genes Chromosomes Cancer. 2016 May;55(5):480-91. doi: 10.1002/gcc.22350. Epub 2016 Feb 23. PMID: 26774012

76) Mikhail FM, Biegel JA, Cooley LD, et al. Technical laboratory standards for interpretation and reporting of acquired copy-number abnormalities and copy-neutral loss of heterozygosity in neoplastic disorders: a joint consensus recommendation from the American College of Medical Genetics and Genomics (ACMG) and the Cancer Genomics Consortium (CGC). Genet Med. 2019 Sep;21(9):1903-1916. doi: 10.1038/s41436-019-0545-7. Epub 2019 May 29. PMID: 31138931

77) Rack KA, van den Berg E, Haferlach C, et al. European recommendations and quality assurance for cytogenomic analysis of haematological neoplasms. Leukemia. 2019 Aug;33(8):1851-1867. doi: 10.1038/s41375-019-0378-z. Epub 2019 Jan 29. PMID: 30696948; PMCID: PMC6756035.

78) Raghavan M, Gupta M, Molloy G, et al. Mitotic recombination in haematological malignancy. Adv Enzyme Regul. 2010;50(1):96-103. doi: 10.1016/j.advenzreg.2009.10.030. Epub 2009 Nov 4. PMID: 19895835

79) Young BD, Debernardi S, Lillington DM, et al. A role for mitotic recombination in leukemogenesis. Adv Enzyme Regul. 2006;46:90-7. doi: 10.1016/j.advenzreg.2006.01.015. Epub 2006 Aug 4. PMID: 16890980

80) Nguyen L, W M Martens J, Van Hoeck A, Cuppen E. Pan-cancer landscape of homologous recombination deficiency. Nat Commun. 2020 Nov 4;11(1):5584. doi: 10.1038/s41467-020-19406-4. PMID: 33149131; PMCID: PMC7643118

81) Pedersen BS, De S. Loss of heterozygosity preferentially occurs in early replicating regions in cancer genomes. Nucleic Acids Res. 2013 Sep;41(16):7615-24. doi: 10.1093/nar/gkt552. Epub 2013 Jun 22. PMID: 23793816; PMCID: PMC3763542

82) Zhang X, Sjöblom T. Targeting Loss of Heterozygosity: A Novel Paradigm for Cancer Therapy. Pharmaceuticals (Basel). 2021 Jan 13;14(1):57. doi: 10.3390/ph14010057. PMID: 33450833; PMCID: PMC7828287

83) Iacobucci I, Mullighan CG. Genetic Basis of Acute Lymphoblastic Leukemia. J Clin Oncol. 2017 Mar 20;35(9):975-983. doi: 10.1200/JCO.2016.70.7836. Epub 2017 Feb 13. PMID: 28297628; PMCID: PMC5455679

*84)* Molina O, Bataller A, Thampi N, et al. Near-Haploidy and Low-Hypodiploidy in B-Cell Acute Lymphoblastic Leukemia: When Less Is Too Much. Cancers (Basel). 2021 Dec 22;14(1):32. doi: 10.3390/cancers14010032. PMID: 35008193; PMCID: PMC8750410

*85)* Schwartz DC, Li X, Hernandez LI, et al. Ordered restriction maps of Saccharomyces cerevisiae chromosomes constructed by optical mapping. Science. 1993 Oct 1;262(5130):110-4. doi: 10.1126/science.8211116. PMID: 8211116

*86)* Bionano Genomics. 30110 Rev K, Bionano Solve Theory of Operation: Structural Variant Calling. 2021

87) Levy, B, Baughn, LB, Chartrand, S, et al. (2020) A national multicentre evaluation of the clinical utility of optical genome mapping for assessment of genomic aberrations in acute myeloid leukemia. medRxiv; 2020; 1-35. doi: 10.1101/2020.11.07.20227728

88) Gerding WM, Tembrink M, Nilius-Eliliwi V, et al. Optical genome mapping reveals additional prognostic information compared to conventional cytogenetics in AML/MDS patients. Int J Cancer. 2022 Jun 15;150(12):1998-2011. doi: 10.1002/ijc.33942. Epub 2022 Feb 7. PMID: 35064925

89) Yang H, Garcia-Manero G, Sasaki K, et al. High-resolution structural variant profiling of myelodysplastic syndromes by optical genome mapping uncovers cryptic aberrations of prognostic and therapeutic significance. Leukemia. 2022 Sep;36(9):2306-2316. doi: 10.1038/s41375-022-01652-8. Epub 2022 Aug 1. PMID: 35915143; PMCID: PMC9417987

90) Giguère A, Raymond-Bouchard I, Collin V, et al. Optical Genome Mapping Reveals the Complex Genetic Landscape of Myeloma. Cancers (Basel). 2023 Sep 22;15(19):4687. doi: 10.3390/cancers15194687. PMID: 37835381; PMCID: PMC10571866

91) Zou YS, Klausner M, Ghabrial J, et al. A comprehensive approach to evaluate genetic abnormalities in multiple myeloma using optical genome mapping. Blood Cancer J. 2024 May 3;14(1):78. doi: 10.1038/s41408-024-01059-x. PMID: 38702349; PMCID: PMC11068911

92) Puiggros A, Ramos-Campoy S, Kamaso J, et al. Optical Genome Mapping: A Promising New Tool to Assess Genomic Complexity in Chronic Lymphocytic Leukemia (CLL). Cancers (Basel). 2022 Jul 11;14(14):3376. doi: 10.3390/cancers14143376. PMID: 35884436; PMCID: PMC9317182

93) Podvin B, Roynard P, Boudry A, et al. Whole-genome optical mapping to elucidate myeloid/lymphoid neoplasms with eosinophilia and tyrosine kinase gene fusions. Leuk Res. 2022 Dec;123:106972. doi: 10.1016/j.leukres.2022.106972. Epub 2022 Oct 21. PMID: 36306722

94) Rack K, De Bie J, Ameye G, et al. Optimizing the diagnostic workflow for acute lymphoblastic leukemia by optical genome mapping. Am J Hematol. 2022 May;97(5):548-561. doi: 10.1002/ajh.26487. Epub 2022 Mar 9. Erratum in: Am J Hematol. 2023 Mar;98(3):543. doi: 10.1002/ajh.26584. PMID: 35119131; PMCID: PMC9314940

95) Brandes D, Yasin L, Nebral K, et al. Optical Genome Mapping Identifies Novel Recurrent Structural Alterations in Childhood ETV6::RUNX1+ and High Hyperdiploid Acute Lymphoblastic Leukemia. Hemasphere. 2023 Jul 17;7(8):e925. doi: 10.1097/HS9.0000000000000925. PMID: 37469802; PMCID: PMC10353714.

96) Xu H, Gao H, Wang C, et al. Optical Genome Mapping Reveals Novel Structural Variants in Lymphoblastic Lymphoma. J Pediatr Hematol Oncol. 2024 Jan 1;46(1):e71-e82. doi: 10.1097/MPH.0000000000002787. Epub 2023 Nov 29. PMID: 38018972

97) Schouten JP, McElgunn CJ, Waaijer R, et al. Relative quantification of 40 nucleic acid sequences by multiplex ligation-dependent probe amplification. Nucleic Acids Res. 2002 Jun 15;30(12):e57. doi: 10.1093/nar/gnf056. PMID: 12060695; PMCID: PMC117299

98) Benard-Slagter A, Zondervan I, de Groot K, et al. Digital Multiplex Ligation-Dependent Probe Amplification for Detection of Key Copy Number Alterations in T- and B-Cell Lymphoblastic Leukemia. J Mol Diagn. 2017 Sep;19(5):659-672. doi: 10.1016/j.jmoldx.2017.05.004. Epub 2017 Jul 19. PMID: 28736295

99) Kiss R, Gángó A, Benard-Slagter A, et al. Comprehensive profiling of disease-relevant copy number aberrations for advanced clinical diagnostics of pediatric acute lymphoblastic leukemia. Mod Pathol. 2020 May;33(5):812-824. doi: 10.1038/s41379-019-0423-5. Epub 2019 Dec 19. PMID: 31857684

100) Thakral D, Kaur G, Gupta R, et al. Rapid Identification of Key Copy Number Alterations in B- and T-Cell Acute Lymphoblastic Leukemia by Digital Multiplex Ligation-Dependent Probe

Amplification. Front Oncol. 2019 Sep 13;9:871. doi: 10.3389/fonc.2019.00871. PMID: 31572674; PMCID: PMC6753626

101)    Zhang XY, Dai HP, Li Z, Yin J, Lang XP, Yang CX, Xiao S, Zhu MQ, Liu DD, Liu H, Shen HJ, Wu DP, Tang XW. Identification of *STRBP* as a Novel *JAK2* Fusion Partner Gene in a Young Adult With Philadelphia Chromosome-Like B-Lymphoblastic Leukemia. Front Oncol. 2021 Jan 11;10:611467. doi: 10.3389/fonc.2020.611467. PMID: 33505919; PMCID: PMC7831028

102)    Tasian SK, Loh ML, Hunger SP. Philadelphia chromosome-like acute lymphoblastic leukemia. Blood. 2017 Nov 9;130(19):2064-2072. doi: 10.1182/blood-2017-06-743252. Epub 2017 Oct 2. PMID: 28972016; PMCID: PMC5680607

103)    Hirabayashi S, Ohki K, Nakabayashi K, et al. ZNF384-related fusion genes define a subgroup of childhood B-cell precursor acute lymphoblastic leukemia with a characteristic immunotype. Haematologica. 2017 Jan;102(1):118-129. doi: 10.3324/haematol.2016.151035. Epub 2016 Sep 15. PMID: 27634205; PMCID: PMC5210242

104)    Gu Z, Churchman M, Roberts K, et al. Genomic analyses identify recurrent MEF2D fusions in acute lymphoblastic leukaemia. Nat Commun. 2016 Nov 8;7:13331. doi: 10.1038/ncomms13331. PMID: 27824051; PMCID: PMC5105166

105)    Roberts KG, Li Y, Payne-Turner D, et al. Targetable kinase-activating lesions in Ph-like acute lymhoblastic leukemia. N Engl J Med. 2014 Sep 11;371(11):1005-15. doi: 10.1056/NEJMoa1403088. PMID: io'r125207766; PMCID: PMC4191900

106)    Emmrich S, Streltsov A, Schmidt F, et al. LincRNAs MONC and MIR100HG act as oncogenes in acute megakaryoblastic leukemia. Mol Cancer. 2014 Jul 15;13:171. doi: 10.1186/1476-4598-13-171. PMID: 25027842; PMCID: PMC4118279

107)    Lühmann JL, Stelter M, Wolter M, et al. The Clinical Utility of Optical Genome Mapping for the Assessment of Genomic Aberrations in Acute Lymphoblastic Leukemia. Cancers (Basel). 2021 Aug 30;13(17):4388. doi: 10.3390/cancers13174388. PMID: 34503197; PMCID: PMC8431583.

108)    Lestringant V, Duployez N, Penther D, et al. Optical genome mapping, a promising alternative to gold standard cytogenetic approaches in a series of acute lymphoblastic leukemias. Genes Chromosomes Cancer. 2021 Oct;60(10):657-667. doi: 10.1002/gcc.22971. Epub 2021 May 26. PMID: 33982372.

109)    Vieler LM, Nilius-Eliliwi V, Schroers R, et al. Optical Genome Mapping Reveals and Characterizes Recurrent Aberrations and New Fusion Genes in Adult ALL. Genes (Basel). 2023 Mar 9;14(3):686. doi: 10.3390/genes14030686. PMID: 36980958; PMCID: PMC10048194

110)    Lew-Derivry L, Marceau-Renaut A, Fenwarth L, et al. Prognostic impact of RUNX1 mutations and deletions in pediatric acute myeloid leukemia: results from the French ELAM02 study group.

Leukemia. 2023 Aug;37(8):1723-1726. doi: 10.1038/s41375-023-01931-y. Epub 2023 Jun 16. PMID: 37328541; PMCID: PMC10400410

111)      Kannan S, Aitken MJL, Herbrich SM, et al. Antileukemia Effects of Notch-Mediated Inhibition of Oncogenic PLK1 in B-Cell Acute Lymphoblastic Leukemia. Mol Cancer Ther. 2019 Sep;18(9):1615-1627. doi: 10.1158/1535-7163.MCT-18-0706. Epub 2019 Jun 21. PMID: 31227645; PMCID: PMC6726528